Heliyon 10 (2024) e28088

Contents lists available at ScienceDirect

Heliyon

journal homepage: www.cell.com/heliyon

Research article

Identification and validation of mutual hub genes in idiopathic pulmonary fibrosis and rheumatoid arthritis-associated usual interstitial pneumonia

Liangyu Chen [a,b], Haobo Lin [c,d,e], Linmang Qin [c,d,e], Guangfeng Zhang [c,d,e], Donghui Huang [b], Peisheng Chen [b], Xiao Zhang [a,f,*]

[a] Faculty of Chinese Medicine, Macau University of Science and Technology, Macau, China
[b] Department of Respiratory and Critical Care Medicine, Zhuhai Hospital of Integrated Traditional Chinese and Western Medicine, Zhuhai, China
[c] Department of Rheumatology, Guangdong Provincial People's Hospital, Guangzhou, China
[d] Guangdong Academy of Medical Sciences, Guangzhou, China
[e] Southern Medical University, Guangzhou, China
[f] Department of Rheumatology, The Eighth Affiliated Hospital, Sun Yat-sen University, Shenzhen, China

ARTICLE INFO

Keywords:
Idiopathic pulmonary fibrosis
Rheumatoid arthritis-associated interstitial lung disease
Rheumatoid arthritis-associated usual interstitial pneumonia
Pulmonary fibrosis
Hub genes
Bioinformatics

ABSTRACT

Objectives: The study aims at exploring common hub genes and pathways in idiopathic pulmonary fibrosis (IPF) and rheumatoid arthritis-associated usual interstitial pneumonia (RA-UIP) through integrated bioinformatics analyses.

Methods: The GSE199152 dataset containing lung tissue samples from IPF and RA-UIP patients was acquired from the Gene Expression Omnibus (GEO) database. The identification of overlapping differentially expressed genes (DEGs) in IPF and RA-UIP was carried out through R language. Protein–protein interaction (PPI) network analysis and module analysis were applied to filter mutual hub genes in the two diseases. Enrichment analyses were also conducted to analyze the possible biological functions and pathways of the overlapped DEGs and hub genes. The diagnostic value of key genes was assessed with R language, and the expressions of these genes in pulmonary cells of IPF and rheumatoid arthritis-associated interstitial lung disease (RA-ILD) patients were analyzed with single cell RNA-sequencing (scRNA-seq) datasets. The expression levels of hub genes were validated in blood samples from patients, specimens of human lung fibroblasts, lung tissue samples from mice, as well as external GEO datasets.

Abbreviations: IPF, idiopathic pulmonary fibrosis; RA, rheumatoid arthritis; UIP, usual interstitial pneumonia; RA-UIP, rheumatoid arthritis-associated usual interstitial pneumonia; ILD, interstitial lung disease; RA-ILD, rheumatoid arthritis-associated interstitial lung disease; GEO, gene expression omnibus; DEGs, differentially expressed genes; PPI, protein–protein interaction; GO, gene ontology; KEGG, kyoto enrichment of genes and genomes; GSEA, gene set enrichment analysis; qRT-PCR, quantitative real-time polymerase chain reaction; IHC, immunohistochemistry; EMT, epithelial mesenchymal transition; STRING, search tool for the retrieval of interacting genes; TGF-β, transforming growth factor-beta; PDGF, platelet-derived growth factor; VEGF, vascular endothelial growth factor; α-SMA, α-smooth muscle actin; COL1A1, collagen I; HLF, human lung fibrosis; MCC, maximal clique centrality; MNC, maximal neighborhood component; EPC, edge percolated component; MF, molecular function; BP, biological process; CC, cellular component; ROC, receiver operating characteristic; TBST, tris-buffered saline with tween; DAB, 3,3′-diaminobenzidine; SEM, standard error of the mean; CI, confidence interval; PBMC, peripheral blood mononuclear cell; DMEM, dulbecco's modified eagle medium; H&E, hematoxylin and eosin; THBS2, thrombospondin 2; TIMP1, metallopeptidase inhibitor 1; POSTN, periostin; ECM, extracellular matrix; MMPs, matrix metalloproteinases; scRNA-seq, single cell RNA-sequencing; PCA, principal component analysis.

* Corresponding author. Faculty of Chinese Medicine, Macau University of Science and Technology, Macau, China.
E-mail address: 13922255387@163.com (X. Zhang).

https://doi.org/10.1016/j.heliyon.2024.e28088
Received 31 October 2023; Received in revised form 8 March 2024; Accepted 12 March 2024
Available online 22 March 2024

Results: Four common hub genes (THBS2, TIMP1, POSTN, and CD19) were screened. Enrichment analyses showed that the abnormal expressions of DEGs and hub genes may be connected with the onset of IPF and RA-UIP by regulating the progression of fibrosis. ScRNA-seq analyses illustrated that for both IPF and RA-ILD patients, THBS2, TIMP1, and POSTN were mainly expressed in lung fibroblasts, while CD19 was uniquely high-expressed in B cells. The qRT-PCR and immunohistochemistry (IHC) results verified that the expression levels of hub genes were mostly in accordance with the findings obtained from the bioinformatics analyses.
Conclusion: Though IPF and RA-UIP are distinct diseases, they may to some extent have mutual pathogenesis in the development of fibrosis. THBS2, TIMP1, POSTN, and CD19 may be the potential biomarkers of IPF and RA-UIP, and intervention on related pathways of these genes could offer new strategies for the precision treatment of IPF and RA-UIP.

1. Introduction

IPF is a progressive and chronic disease featuring usual interstitial pneumonia (UIP) on imaging and histopathology, the etiology of which remains unexplained [1]. Rheumatoid arthritis (RA) is an illness distinguished by the presence of erosive and inflammatory synovitis. Interstitial lung disease (ILD) is a typical extra-articular manifestation of RA. Among all patterns of RA-ILD, UIP is the most prevalent type [2]. Though IPF and RA-ILD are separate diseases, they share similar clinical manifestations, imaging characteristics, and genetic features [3]. Recently, researchers have found that they have some associations in pathogenesis. For instance, the functional MUC5B rs35705950 promoter variant, along with the mutation of some telomere maintenance genes, have been considered as the common genetic risk factors for IPF and RA-ILD [4]. The development of the 2 diseases can also be regulated by several biological pathways, such as JAK/STAT signaling pathway, 5-HT pathway, and citrullination pathway [5–7]. More importantly, both diseases could develop into UIP [3].

UIP, a common pattern of pulmonary fibrosis in fibrotic ILDs, is histopathologically characterized by accumulation of extracellular matrix (ECM), abnormality of alveolar re-epithelialization, proliferation of lung fibroblasts, and transdifferentiation from fibroblasts to myofibroblasts [8,9]. In recent years, it's been recognized that UIP is mainly caused by maladaptive repair of recurrently injured lung epithelium and pathological dysfunction of pulmonary fibroblasts [8]. Under normal conditions, alveolar type 2 cells are able to repair micro-injuries, and lung fibroblasts maintain the structure and function of lung tissue. However, due to factors like gene mutations and aging, dysfunctional type 2 cells can develop aberrant behaviors, leading to the synthesis and secretion of cytokines such as TGF-β, PDGF, and VEGF, which stimulate epithelial mesenchymal transition (EMT) and induce fibrotic processes [10]. Meanwhile, abnormal fibroblasts actively respond to these fibrosis-related cytokines, thus accelerating differentiation into myofibroblasts and producing excessive amounts of collagen and other ECM components [11]. Such pathological alterations are characteristic signs of pulmonary fibrosis.

The onset and progression of UIP are regulated by a variety of factors. Among these, TGF-β is widely recognized as one of the most crucial triggers. This cytokine promotes lung fibroblast-to-myofibroblast transition, resulting in the overexpression of α-smooth muscle actin (α-SMA) and collagens. Therefore, TGF-β is frequently used to incubate human lung fibroblasts (HLFs) for constructing the in vitro model of pulmonary fibrosis [12]. Furthermore, UIP can be induced by several types of medicine, and the most typical one is bleomycin. This drug used for neoplasms has been proven to have lung toxicity, as it provokes pulmonary interstitial inflammation, alveolar epithelium injuries, and epithelial-mesenchymal transition [13]. However, the severe side effects never limit its experimental applications, for the mouse models induced by bleomycin are widely employed to simulate the histopathological states of UIP patients. Researchers using mouse models of bleomycin-induced pulmonary fibrosis have discovered many mechanisms of IPF and other fibrotic ILDs [14].

Nowadays, we still don't fully understand the pathological mechanisms of IPF and RA-UIP. Exploring the common hub genes in IPF and RA-UIP through bioinformatics analysis may contribute to further comprehending their mutual biological pathways. Our research offers insights into the underlying genetic mechanisms and therapeutic targets of the 2 diseases.

2. Materials and methods

2.1. Data collection

The raw mRNA data of the fresh frozen lung tissue samples from 20 IPF patients, 3 RA-UIP patients, and 4 non-UIP controls was acquired from the GSE199152 dataset available on the GEO database. The sequencing of these samples was performed utilizing the GPL16791 platform.

2.2. Data extraction for DEGs

The identification of DEGs between IPF and non-UIP samples, as well as between RA-UIP and non-UIP samples, was conducted using the "DESeq2″ R package—a tool designed for the differential analysis of high-throughput sequencing data. "DESeq2" enhances the stability and interpretability of estimates utilizing shrinkage estimation for dispersions and fold changes, though it has limitations

such as sensitivity to small sample sizes, possibility of long computation times, and difficulties with zero counts and low-expressed genes [15]. After inputting raw gene count data, normalizing data, estimating gene-wise dispersion, and performing statistical tests for differential expression, the DEGs were determined by a standard of a p-value less than 0.05 and |logFC| greater than 1. For visual representation, volcano plots and heatmaps were created to illustrate the DEGs. Subsequently, the Venn diagram was employed to investigate the overlapping DEGs between IPF and RA-UIP.

2.3. PPI network establishment and module analysis

In order to build a PPI network, the overlapped DEGs were imported into the Search Tool for the Retrieval of Interacting Genes (STRING, version: 11.5) and then visualized using Cytoscape software. Cytoscape is an open-source platform for visualizing and analyzing complex networks [16]. It offers a wide range of analysis tools and algorithms for PPI network analysis, module identification, and hub gene selection. CytoHubba, a plugin integrated into Cytoscape, was employed to filter hub genes, utilizing seven different analytical methods: maximal clique centrality (MCC), maximal neighborhood component (MNC), edge percolated component (EPC), degree, closeness, radiality, and bottleneck. The top 10 genes filtered by each method were selected, and those that overlapped between these methods were identified as core genes. [17,18]. MCODE is another plugin within Cytoscape software for the purpose of module analysis and hub gene identification [18]. Modules of interest were decided with specific criteria, including a degree cutoff of 2, a K-core value of 2, and a node score cutoff of 0.3.

2.4. Gene ontology (GO) and kyoto enrichment of genes and genomes (KEGG) analyses

GO and KEGG enrichment analyses were implemented to analyze the biological activities of the overlapping DEGs and hub genes in IPF and RA-UIP through the "ClusterProfiler" R package. GO and KEGG analyses are bioinformatics tools to categorize genes and proteins according to their functions and biological processes, and to map them onto predefined systemic pathways and networks, enhancing our understanding of their roles in complex biological mechanisms [19,20]. GO analysis was conducted to discover the biological processes (BP), cellular components (CC), and molecular functions (MF), while the application of KEGG analysis was used to investigate signal pathways associated with mutual DEGs and key genes. The predetermined level of statistical significance was a p-value below 0.05, and the top 8 enriched categories were visualized through barplots and dotplots.

2.5. Gene set enrichment analysis (GSEA) utilization

According to the median expression values of each hub gene, IPF and RA-UIP patients were respectively divided into high-expression and low-expression groups. GSEA, a tool that uses functional categories to compute the enrichment score of gene sets and explore diverse functional phenotypes [21], was employed to distinguish the biological pathways between the high-expression and low-expression groups. With this approach using "ClusterProfiler" R package, hub genes and other related expressed genes would be categorized into specific gene sets that may be relevant to the pathogenesis of IPF and RA-UIP. To investigate the mutual biological processes in IPF and RA-UIP, the enriched gene sets of each hub gene that overlapped between the two diseases were regarded as the common potential biological pathways. Significant enrichment was determined for p-values <0.05.

2.6. Diagnostic value of hub genes

Applying the "pROC" R package, a method for visualizing and analyzing the diagnostic performance through receiver operating characteristic (ROC) curves [22], the ROC analysis was executed to assess the ability of core genes to differentiate IPF or RA-UIP samples from normal samples. This analysis provides significant insights into the diagnostic power of hub genes and their potential utility in clinical practice.

2.7. Analysis of single cell RNA-sequencing (scRNA-seq) data

To further comprehend the roles of hub genes in specific types of pulmonary cells in IPF and RA-UIP patients, we performed scRNA-seq analyses on datasets GSE213017 and GSE180139 with the use of R package "Seurat" [23]. GSM6568651 in GSE213017 and GSM5454350 in GSE180139 were selected as analytical objects, for they respectively contained single cell RNA-sequencing data of pulmonary cells of an IPF patient and a RA-ILD patient. It should be noted that the RA-ILD patient in GSM5454350 simultaneously suffered from lung cancer, but it's the one and only scRNA-seq data of RA-ILD patient we could obtain on GEO database by far. Quality control (200 $<$number of feature RNA $<$2500, percentage of mitochondrial genes $<$15%) was conducted in the 2 objects, and the NormalizeData function in "Seurat" package was employed to normalize the scRNA-seq data. Seurat Principal Component Analysis (PCA) instruction was subsequently run for dimension reduction, and RunTSNE function in "Seurat" package was utilized for cell clustering. "FindAllMarkers" instruction within "Seurat" package was then applied to compute gene markers for each cell cluster, which were distinguished by PanglaoDB [24] and CellMarker database [25] and used for cell type annotation. The relative expressions of hub genes in each classified cell type were visualized through dotplot, violinplot, and featureplot. In addition, the top 200 high expressed genes in lung fibroblasts of each sample were differentiated by "FindAllMarkers" function, and the intersected top high-expressed genes in fibroblasts between the 2 samples were acquired through a Venn diagram. Moreover, KEGG and GO analyses were implemented to predict the functions of these mutual top high-expressed genes in lung fibroblasts. The p-values below 0.05 were deemed significant.

2.8. Validation of hub genes through qRT-PCR

We collected peripheral blood from 18 patients that were divided into 3 groups: 6 IPF patients in the IPF group, 6 RA-UIP patients in the RA-UIP group, and 6 healthy controls in the control group. All research subjects were recruited at the Guangdong Provincial People's Hospital from March 2023 to August 2023. The IPF patients were selected via diagnostic criteria of IPF established by ATS/ERS/JRS/ALAT clinical guideline [26], while RA-UIP patients were diagnosed by the RA classification criteria provided by the American College of Rheumatology/European League against Rheumatism [27] and met the radiological and histopathological features of the definite UIP pattern based on ATS/ERS/JRS/ALAT guideline [26]. Table S1 displays the characteristics of the samples. There were no statistical differences in gender or age among the 3 groups (Table 1). Ficoll-Paque PREMIUM (Amresco, USA) was applied to separate peripheral blood mononuclear cells (PBMCs) from the donors' blood. The total RNA of PBMC specimens was isolated with Trizol reagent (Thermofisher, USA).

We obtained lung tissues from lung cancer patients who underwent lobectomies in the Department of Thoracic Surgery, Guangdong Provincial People's Hospital. The lung tissues were proved healthy through biopsy and were more than 5 cm away from the lesion sites. These tissues were cut into 1 mm^3 pieces, evenly distributed in culture dishes, and then placed upside down in a 37 °C and 5% CO2 incubator. 4 h later, the pieces were attached to the bottom of the dishes, which were then turned over and added with high-glucose Dulbecco's Modified Eagle Medium (DMEM, Thermofisher, USA) including 20% fetal bovine serum (ZETA LIFE, USA) and 1% penicillin-streptomycin cocktail. The primary human lung fibroblasts were extracted when they crawled out of the tissues and became colonies. After being cultured for 4–6 passages, fibroblasts extracted from the patients were subcultured into two 60-mm culture dishes and divided into 2 groups. One group served as control group and the other as in vitro model group. Both dishes were incubated with DMEM containing 10% fetal bovine serum and 1% penicillin-streptomycin cocktail until the cell density reached 60%. The control group dish was subsequently replaced with fresh medium, while the dish in model group was incubated with fresh medium and 10 ng/ml TGF-β1 (PEPROTECH, USA) for 48 h. After that, total RNA of fibroblasts in each dish was extracted with Trizol reagent (Thermofisher, USA). The experiment was run in triplicate to ensure that each group had 3 total RNA samples of fibroblasts from different batches.

The RNA of PBMC specimens and fibroblast samples was separately synthesized into complementary DNA with the Evo M-MLV Reverse Transcriptase Premix Kit (Agbio, China). And qRT-PCR was run on a qTOWER real-time qPCR system (Analytik Jena, Germany) with the SYBR Green Premix Pro Taq HS qPCR kit (Agbio, China). GAPDH was used as an internal normalization standard. The $2^{-\triangle\triangle Ct}$ method was utilized to calculate the mRNA expression levels of genes of interest. Sequences of the primers are detailed in Table 2.

2.9. Validation of hub genes through immunohistochemistry

At the Laboratory Animal Research Center of South China University of Technology, we raised twelve 8-week-old male C57BL/6J mice and randomly split them into a control group and a bleomycin model group, with 6 in each. The procedure began with anaesthetizing the mice through intraperitoneal injection of pentobarbital sodium solution (50 mg/kg), followed by securing their limbs and tilting their heads upwards. Using forceps, their epiglottides were then exposed, and the model group mice were instilled with bleomycin solution (3 mg/kg) into the trachea to induce pulmonary fibrosis, while the controls underwent intra-tracheal injection of equivalent volume of saline. 14 days later, the mice were euthanized for lung tissue hematoxylin and eosin (H&E) staining and immunohistochemical staining.

For H&E staining, mouse lung tissue samples were paraffin-embedded, sectioned at 4 μm, deparaffinized, stained with hematoxylin and eosin, sealed, and then observed under a microscope(CX31, Olympus, Japan). For immunohistochemical staining, mouse lung tissue specimens were embedded in paraffin, then sliced consistently and evenly into sections of 4 μm in thickness, followed by the removal of paraffin transitioning the samples to an aqueous state. These sections were later soaked in 3% hydrogen peroxide for 20 min and blocked in 10% normal goat serum for 20 min after antigen retrieval was completed. Antibody incubation was conducted overnight at 4 °C using the primary antibodies listed in Table 3. Subsequent to 3 washes in tris-buffered saline with tween (TBST), each slide was incubated with corresponding secondary antibodies as indicated in Table 3, maintained at 37 °C for a duration of 45 min. Following this incubation period, the slices were again washed 3 times using TBST. The color was generated using 3, 3′-Diaminobenzidine (DAB), examined through a microscope (CX31, Olympus, Japan), and captured in photographs.

Images were next exported to ImageJ software for further analysis. The IHC Toolbox plugin (download at http://rsb.info.nih.gov/ij/plugins/ihc-toolbox/index.html) in ImageJ software facilitated the detection and extraction of the brown DAB-stained regions, which were regarded as positive immunostained areas [28]. The proportion of immunostained areas was utilized as a quantitative

Table 1
Clinicopathological variables of cases and controls.

Variables	Groups			P-value
	IPF(n = 6)	RA-UIP(n = 6)	Control(n = 6)	
Age (years)	65.50 ± 3.757	63.67 ± 3.712	56.50 ± 6.722	0.4167
Gender (male/female)	5/1	3/3	4/2	0.818

Notes: The data are presented in the form of mean ± standard error of the mean (SEM). P-values were calculated utilizing Analysis of Variance (ANOVA) or Fisher's exact test.

Table 2
Primer information.

Target name	Primer		Species
GAPDH	F	GTCTCCTCTGACTTCAACAGCG	Human
	R	ACCACCCTGTTGCTGTAGCCAA	
THBS2	F	CAGTCTGAGCAAGTGTGACACC	Human
	R	TTGCAGAGACGGATGCGTGTGA	
TIMP1	F	GGAGAGTGTCTGCGGATACTTC	Human
	R	GCAGGTAGTGATGTGCAAGAGTC	
POSTN	F	CAGCAAACCACCTTCACGGATC	Human
	R	TTAAGGAGGCGCTGAACCATGC	
CD19	F	CCCAAGGGGCCTAAGTCATTG	Human
	R	AACAGACCCGTCTCCATTACC	
α-SMA	F	CTATGCCTCTGGACGCACAACT	Human
	R	CAGATCCAGACGCATGATGGCA	
COL1A1	F	GATTCCCTGGACCTAAAGGTGC	Human
	R	AGCCTCTCCATCTTTGCCAGCA	

Table 3
Antibody information.

Name	Type	Source	Identifier	Species	Concentration
THBS2	Primary antibody	Boster/China	BA3616-2	Rabbit	1:100
TIMP1	Primary antibody	Affinity/China	AF7007	Rabbit	1:100
POSTN	Primary antibody	Proteintech/China	19899-1-AP	Rabbit	1:800
CD19	Primary antibody	Abcam/Britain	ab245235	Rabbit	1:1000
α-SMA	Primary antibody	Abcam/Britain	ab7817	Mouse	1:6000
COL1A1	Primary antibody	Boster/China	BA0325	Rabbit	1:500
Gout anti-Rabbit IgG	Secondary antibody	Abcam/Britain	ab205718	–	1:2000
Gout anti-Mouse IgG	Secondary antibody	Abcam/Britain	ab205719	–	1:2000

measure to assess and compare the expression levels of interested proteins between mice in the bleomycin group and the control group. The result was analyzed and visualized with scatter plots using GraphPad PRISM 8 software, considering a p-value less than 0.05 as indicative of statistical significance.

2.10. Validation of hub genes through external GEO datasets

We then validated the core genes with external GEO datasets GSE150910 and GSE89408. The mRNA sequencing data of lung tissues from 103 IPF patients and 103 controls in GSE150910 dataset was selected for validation. In addition, as we couldn't find any other mRNA sequencing datasets involving RA-UIP patients, the GSE89408 dataset containing mRNA data of joint synovial tissues from 152 RA patients and 28 controls was used to examine the expressions of hub genes in general RA patients. Expression data of hub genes for each sample were normalized with log2-trasformation. Boxplots were drawn to compare the relative expression levels of hub genes between patients and controls through GraphPad PRISM 8 software. A p-value less than 0.05 was regarded as statistically significant.

2.11. Statistical analysis

T-test and Analysis of Variance (ANOVA) were used for measurement data (presented as mean ± SEM), whereas Fisher's exact test was used for categorical data. Data were analyzed with R v4.3.1 software, SPSS Statistics 26.0 software, and GraphPad PRISM 8 software. Statistical significance was determined as p less than 0.05.

3. Results

3.1. Identification of mutual DEGs in IPF and RA-UIP

By defining the cut-off value as P less than 0.05 and |logFC| greater than 1, 2537 DEGs between IPF and non-UIP controls were identified. Among these, 1463 genes were found upregulated, while 1074 genes were downregulated. As for RA-UIP, a total of 247 DEGs were detected, with 165 exhibiting upregulation and 82 displaying downregulation. Volcano plots for the DEGs were established by "ggplot2" R package (Fig. 1A and B). The DEGs were also presented with "heatmap" R package (Fig. 1C–D). Venn analysis identified

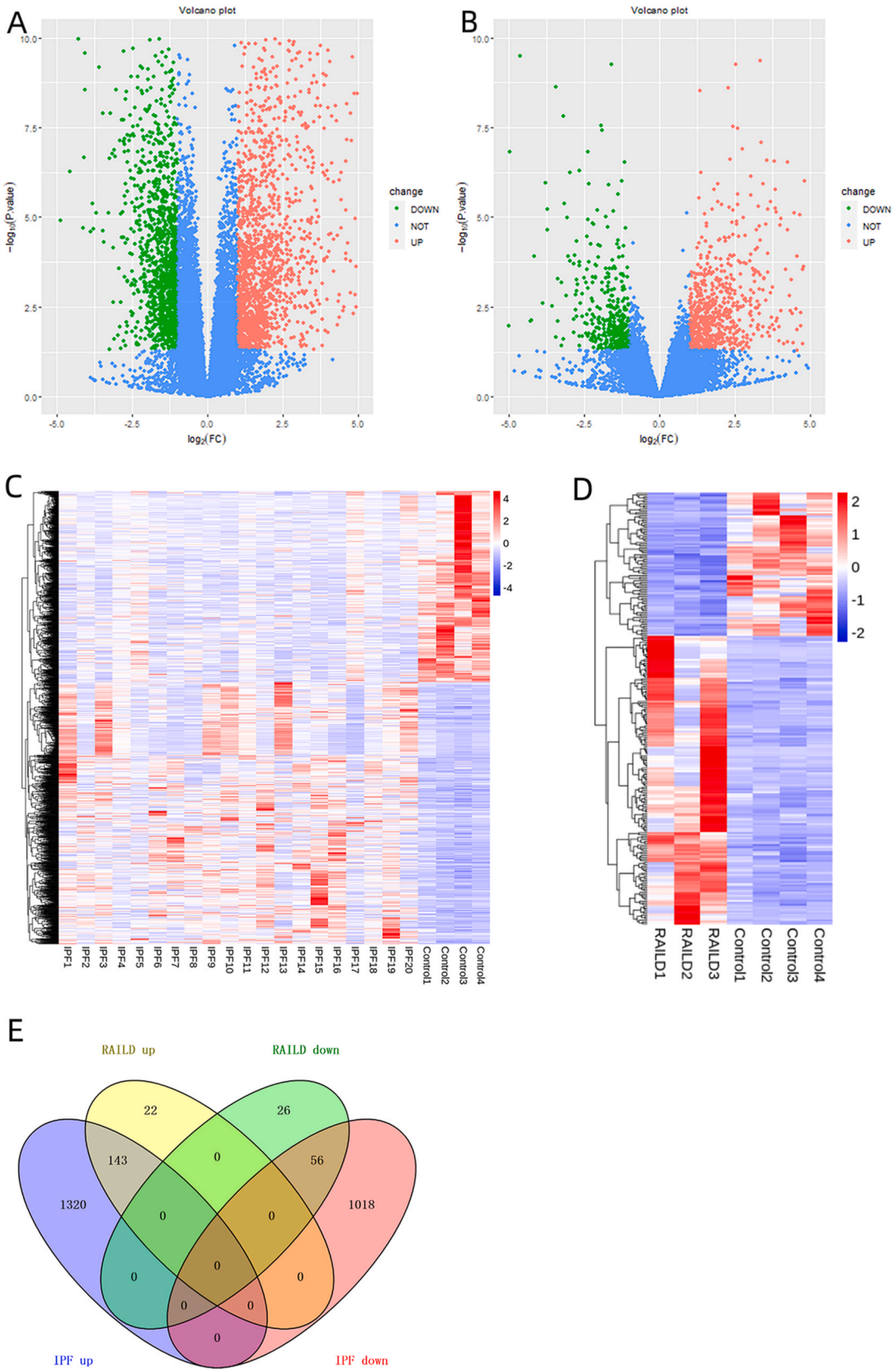

(caption on next page)

Fig. 1. Identification of DEGs. (A).Volcano plot of screening DEGs between IPF patients and non-UIP control individuals. (B).Volcano plot of screening DEGs between RA-UIP patients and non-UIP control individuals. (C).Heatmap of DEGs between IPF patients and non-UIP control individuals. (D)Heatmap of DEGs between RA-UIP patients and non-UIP control individuals. The color red is indicative of a high level of expression, whereas the color blue is indicative of a low level of expression. (E). Venn graph analysis intersected 143 upregulated and 56 downregulated common DEGs in IPF group and RA-UIP group.

199 overlapped DEGs in the two diseases, including 143 upregulated and 56 downregulated genes (Fig. 1E and Table 4).

3.2. Establishment of PPI network and identification of hub gene

We constructed a PPI network with an online database STRING after setting homo sapien as a model organism, and the outcomes were then imported into Cytoscape software (3.9.1) to further filter hub genes. The PPI network dataset comprised 129 nodes and 328 edges (Fig. 2A). Through the seven algorithms of cytoHubba plugin, the top 10 candidate hub genes of each method were calculated (Table 5). After taking the intersection of genes computed by the seven methods, we obtained four common hub genes, including THBS2, TIMP1, POSTN, and CD19, all of which were differentially highly expressed. Module analysis was subsequently conducted using the MCODE plugin within the Cytoscape software. The four hub genes were all in Module 1, which had the highest MCODE score (9.000) and consisted of 27 nodes and 117 edges (Fig. 2B).

3.3. GO and KEGG analyses of common DEGs and hub genes

Based on the filtering standard of adj.p < 0.05, functional characterization of common DEGs was executed through GO analysis, with results visualized in Fig. 3A–D. Predominant BP pathways were pertinent to ECM organization, extracellular structure organization, external encapsulating structure organization, transmembrane receptor protein serine, collagen fibril organization, mesenchymal cell development and differentiation, and connective tissue development. Examination of CC revealed a remarkable enrichment of collagen-containing ECM, external side of plasma membrane, collagen and related complexes, basement membrane, and dense core granule. In terms of MF, activities related to the ECM structural constituent, activities correlated with metalloproteinases, carboxypeptidase activity, platelet-derived growth factor binding, Wnt-protein binding, and protease binding, stood out as significantly enriched. Complementary to this, KEGG analysis presented a notable enrichment of DEGs in pathways connected to ECM-receptor interactions, protein digestion and absorption, as well as the PI3K-Akt signaling pathway.

GO and KEGG analyses were also carried out to characterize the functions of the 4 hub genes, and the results were presented in Fig. 3E–H. Enriched BP pathways included those related to cellular response to ultraviolet, negative regulation of metallopeptidase activity, trophoblast cell migration, integrin pathway regulation, inflammatory responses, and connective tissue replacement. CC analysis suggested that the collagen-containing ECM, platelet granules, and basement membrane were the most enriched cell components. MF analysis highlighted growth factor activity, heparin binding, ECM integrity, and inhibitory activities of metalloendopeptidase, peptidase and endopeptidase as the most enriched molecular functions. As for KEGG pathway analysis, the hub genes were primarily enriched in immunodeficiency, B cell receptor signaling pathway, hematopoietic cell lineage, and HIF-1 signaling pathway.

3.4. GSEA results of hub genes

To further discover the potential biological functions of the four hub genes, GSEA was executed (Date: March 15th, 2023) to distinguish the differentially biological pathways between the high-expression and low-expression groups of each hub gene and to identify the mutual signaling pathways in IPF and RA-UIP. The GSEA revealed that the hub genes exhibited involvement in common related pathways between IPF and RA-UIP, as indicated in Table 6. Enrichment plots of each hub gene in both diseases are shown in Fig. 4A–H.

Table 4
The common DEGs in IPF and RA-UIP

DEGs	Gene symbol
Upregulated Common DEGs	*POSTN; PRG4; GJB2; EBF3; LUZP2; THY1; SULF1; FRZB; WT1; THBS2; TNFRSF9; VCAM1; CTHRC1; EPHA3; COL10A1; PLA2G2A; CR2; UPK1B; IRF4; MEOX1; CPXM2; MMP11; FCRLA; TIMP1; BNC1; PLVAP; RUNDC3B; C1R; CBLN4; UBD; LOC100507421; PAMR1; TNN; VAT1L; CD28; CILP2; ALPK2; CPB1; GNG4; PCP4; ADAMTS18; LINC00473; NR5A2; DSC3; IL13RA2; COL15A1; SLAMF7; ANKRD36BP2; PIM2; SDS; C18orf34; LINC00152; MS4A1; CST2; WT1-AS; CPXM1; CPNE5; LOXL1; ASPN; TLR10; SAMD11; MYRIP; CD19; NRARP; LAX1; P2RY6; CXCL13; ANGPT2; NAV3; COMP; PYCR1; DERL3; SMOC2; CD79A; GREM1; CILP; KIAA1644; C19orf26; C7orf10; MSC; GZMK; TGFB3; WISP1; CADPS; CPA4; LOC375295; SCG2; DNAJC22; ADAMDEC1; KRT6A; CHRDL2; ELFN1; C1S; COL3A1; PSAT1; FLJ41200; AIM2; ROR2; PNOC; LOC100507254; IER5L; PRRX1; FCRL5; KIAA0125; IGFL2; OAF; CLDN1; COL1A1; DIO2; HAPLN3; POU2AF1; CD180; COL1A2; LEF1; SLC1A4; XBP1; SERPINF1; SLAMF1; ABCB1; MZB1; TUBB3; WNT10A; OLFM1; DUSP5; LAMP5; TACR1; TMEM156; IGLL5; NTS; TNFRSF17; FAM46C; SFRP4; BDKRB1; DARC; SERPINE2; MIR650; UAP1; C13orf33; FHL2; PTGFRN; CCR7; FDCSP; FKBP11.*
Downregulated Common DEGs	*NTM; SYN2; TNR; CITED2; CD300LG; LTK; ARRDC2; SEMA3G; NOSTRIN; TMEM100; FOS; MOGAT1; ADRB1; PITPNM2; VIPR1; DUSP1; PRSS21; HSPA12B; CYP1A2; HPCAL4; GPIHBP1; ITGA10; MIR4530; PRX; NXF3; LOC400550; SLC9A3R2; DSCR6; PSORS1C3; NOTCH4; TMPRSS6; TAL1; ALPPL2; BTNL9; HIF3A; TMSB15A; SP6; GRIA1; FOXF1; CLDN5; ACE; CHRM1; RXRG; C20orf160; FAM107A; HECW2; MAP4K2; KLRC3; MPP3; TKTL1; KIR2DL3; NIM1; C2orf91; GRM8; RMST; GNLY.*

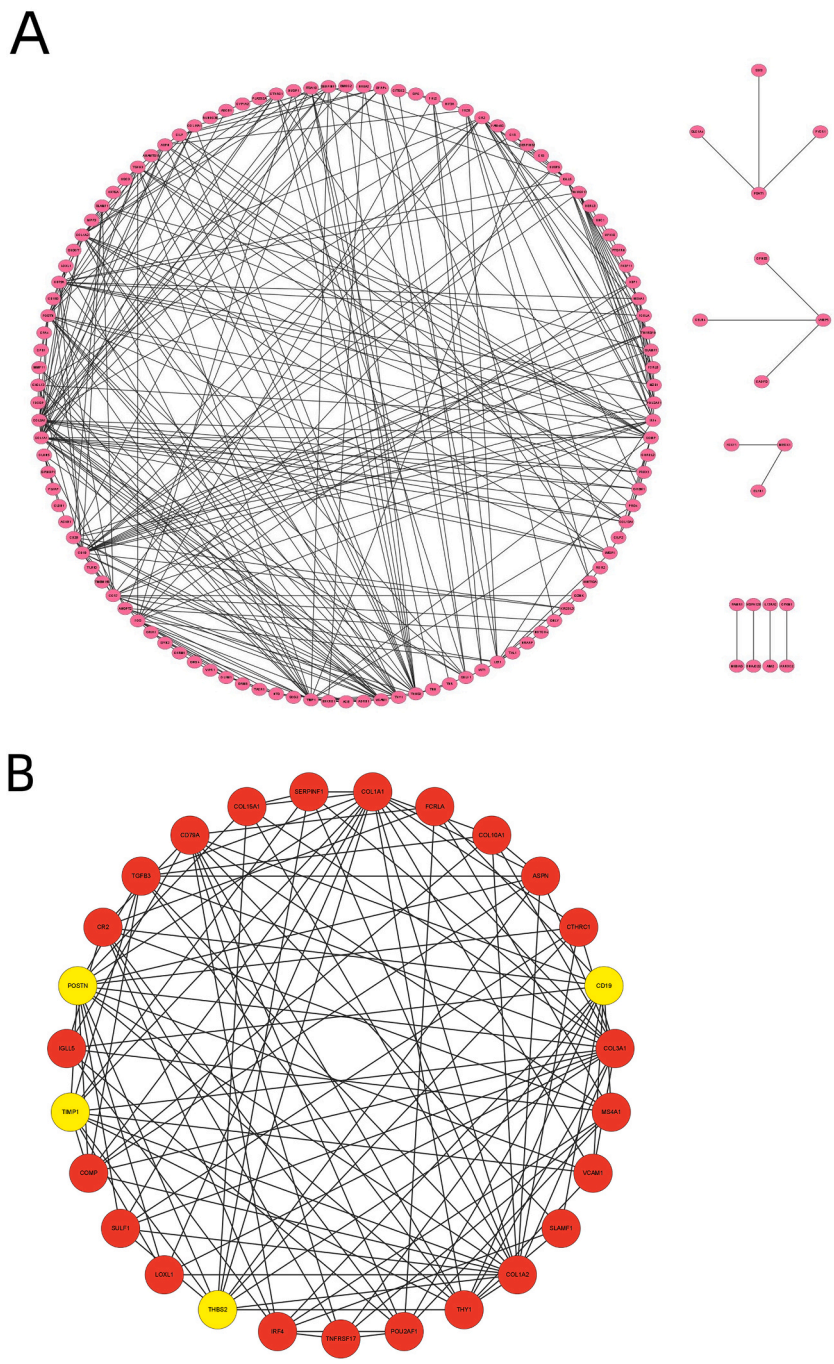

Fig. 2. Visualization of networks. (A).PPI network constructed with the common DEGs. (B).Gene interaction network of the most significant module in MCODE. Highlighted in yellow circles, THBS2, TIMP1, POSTN and CD19 were all in the network.

3.5. Diagnostic evaluation of hub genes

To investigate the diagnostic value of THBS2, TIMP1, POSTN, and CD19 for IPF and RA-UIP, ROC curves were drawn with the expressions of the four core genes to evaluate the accuracy of their diagnostic features employing "pROC" R package (Fig. 5A–B). The AUC values of the core genes greater than 0.7 were considered diagnostically significant. The AUC values of THBS2, TIMP1, POSTN, and CD19 in predicting the diagnostic value of IPF were 0.921 (95% confidence interval (CI), 0.816–1.000), 0.836 (95% CI, 0.658–1.000), 0.929 (95% CI, 0.829–1.000), and 0.779 (95% CI, 0.504–1.000). Meanwhile, the AUC values of THBS2, TIMP1, POSTN, and CD19 for predicting RA-UIP were 0.681 (95% CI, 0.481–0.880), 0.514 (95% CI, 0.310–0.718), 0.694 (95% CI, 0.497–0.892), and

Table 5
Top 10 candidate hub genes in cytoHubba.

Rank	Algorithms in cytoHubba.						
	MCC	MNC	Degree	EPC	BottleNeck	Closeness	Radiality
1	*COL1A1*	*COL1A1*	*COL1A1*	*COL1A1*	*VCAM1*	*COL1A1*	***TIMP1***
2	*COL3A1*	*COL3A1*	*COL3A1*	*COL3A1*	*FOS*	***TIMP1***	*VCAM1*
3	*COL1A2*	***CD19***	***CD19***	*COL1A2*	***CD19***	*COL3A1*	*FOS*
4	***POSTN***	*COL1A2*	*COL1A2*	***POSTN***	***TIMP1***	***CD19***	*THY1*
5	*TGFB3*	***POSTN***	***TIMP1***	***TIMP1***	***THBS2***	*VCAM1*	*COL1A1*
6	***TIMP1***	***TIMP1***	***THBS2***	***THBS2***	***POSTN***	*COL1A2*	*COL3A1*
7	*COMP*	***THBS2***	***POSTN***	*THY1*	*LEF1*	*FOS*	***POSTN***
8	***THBS2***	*IRF4*	*IRF4*	***CD19***	*ANGPT2*	***POSTN***	*TGFB3*
9	***CD19***	*VCAM1*	*FOS*	*VCAM1*	*CD28*	***THBS2***	***THBS2***
10	*CD79A*	*CD79A*	*CCR7*	*TGFB3*	*CLDN5*	*THY1*	***CD19***

Note: The common hub genes were marked in bold.

0.569 (95% CI, 0.115–1.000). In general, the 4 hub genes may possess diagnostic utility in the identification of IPF, but may not be effective diagnostic markers for RA-UIP.

3.6. scRNA-seq analysis

The results of scRNA-seq analysis indicated that for both IPF and RA-ILD patients, THBS2 was specially upregulated in lung fibroblasts, while CD19 was uniquely high-expressed in B cells. Notable upregulation of POSTN was also detected in fibroblast cluster, even though its expression in endothelial cells was similarly significant. TIMP1 expressed in different types of pulmonary cells, but it was observed remarkably high-expressed in fibroblasts (Fig. 6A–H). After intersecting the top 200 highly expressed genes in lung fibroblasts of IPF and RA-ILD patients, a total of 110 overlapped genes were obtained (Fig. 6I and Table 7). GO and KEGG analyses showed that these common top high-expressed genes in lung fibroblasts mainly function in the organization and assembly of extracellular components, muscle function and development, and cellular responses (Fig. 6J–K).

3.7. Expression verification of Hub Genes

To examine the reliability of the hub genes in IPF and RA-UIP patients, the relative mRNA expression levels of core genes were next identified by qRT-PCR in clinical samples. The research data illustrated that mRNA expression levels of THBS2, POSTN, and CD19 were remarkably increased in PBMC specimens of IPF and RA-UIP patients compared with those of controls, whereas the mRNA expression levels of TIMP1 demonstrated no statistical difference either between the IPF and control groups or between the RA-UIP and control groups (Fig. 7A–H).

In terms of cellular experimentation, the in vitro cellular model of pulmonary fibrosis was successfully established, as evidenced by the upregulation of mRNA levels of α-SMA and COL1A1 in the TGF-β1-stimulated group. This implies that TGF-β1 induces fibrogenic responses in lung fibroblasts. Within this framework, the mRNA expression levels of THBS2, TIMP1, POSTN, and CD19 in the TGF-β1-stimulated group exhibited a marked upregulation relative to the control group (Fig. 7I), thus reinforcing the dependability of these hub genes as biomarkers of lung fibrosis.

H&E staining revealed that the lung tissue of the control group mice was normal and healthy, with no noticeable structural impairments. Conversely, bleomycin-induced mice exhibited disordered lung structure, with thickening of alveolar walls, compromised alveoli, inflammation in interstitium, and fibrous tissue accumulation (Fig. 7J). Immunohistochemistry analysis demonstrated a statistically significant increase in the expressions of α-SMA and COL1A1 proteins in the lungs of bleomycin-induced mice (Fig. 7J), confirming the formation of the pulmonary fibrosis animal model. Under the circumstances, proteins such as THBS2, TIMP1, POSTN, and CD19 were significantly upregulated in the model mice (Fig. 7J–K), thus providing additional evidence for the significance of the key genes in lung fibrosis from the perspective of protein expression.

We further validated the hub genes with the external GEO datasets GSE150910 and GSE89408. All of the key genes demonstrated significantly high expressions in IPF patients and RA patients according to the verification datasets (Fig. 7L-M), which suggested that THBS2, TIMP1, POSTN, and CD19 were not only upregulated in IPF and RA-UIP patients, but in patients with general RA.

4. Discussion

Because of the poor efficacy of treatment for the two diseases and their rising prevalence, IPF and RA-UIP have caused severe damage to public health and are still well acknowledged as “incurable”. Therefore, the study on the pathogenesis and genetic mechanisms of IPF and RA-UIP is of far-reaching importance. In this research, the common core genes and related pathways of IPF and RA-UIP were explored through bioinformatics analyses. THBS2, TIMP1, POSTN, and CD19 were upregulated in both IPF and RA-UIP patients and identified as hub genes.

THBS2 (Thrombospondin 2) is a gene that encodes an anti-angiogenic matricellular protein that is recognized as an ECM-modifying enzyme. The THBS2 protein has a substantial role in facilitating the proliferation, migration, and invasion of tumor cells [29]. It has

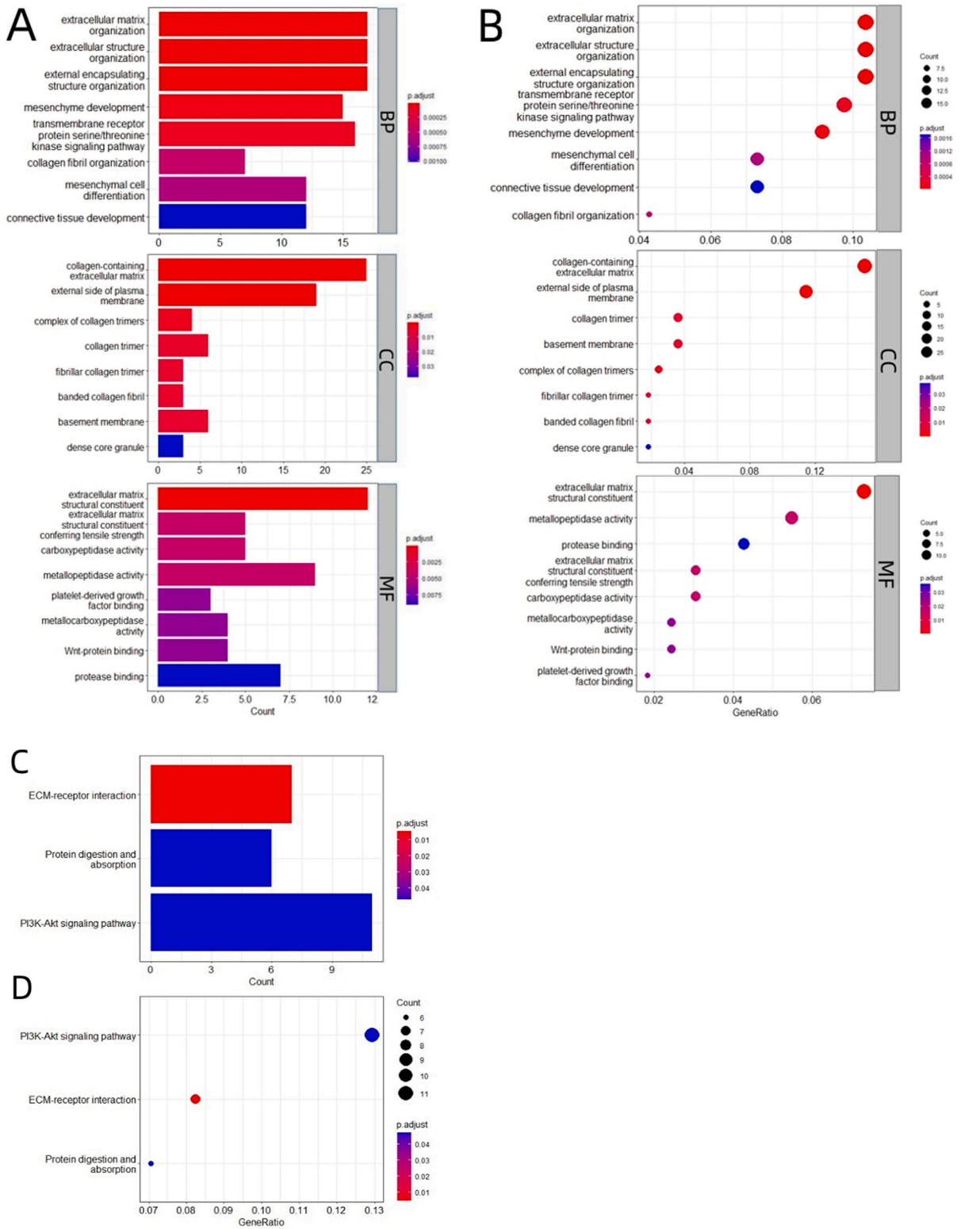

Fig. 3. Enrichment analyses of the mutual DEGs and hub genes. (A).Barplot of GO analysis of the mutual DEGs. (B).Dotplot of GO analysis of the mutual DEGs. (C).Barplot of KEGG analysis of the mutual DEGs. (D).Dotplot of KEGG analysis of the mutual DEGs. (E). Barplot of GO analysis of the 4 hub genes. (F). Dotplot of GO analysis of the 4 hub genes. (G). Barplot of KEGG analysis of the 4 hub genes. (H). Dotplot of KEGG analysis of the 4 hub genes.

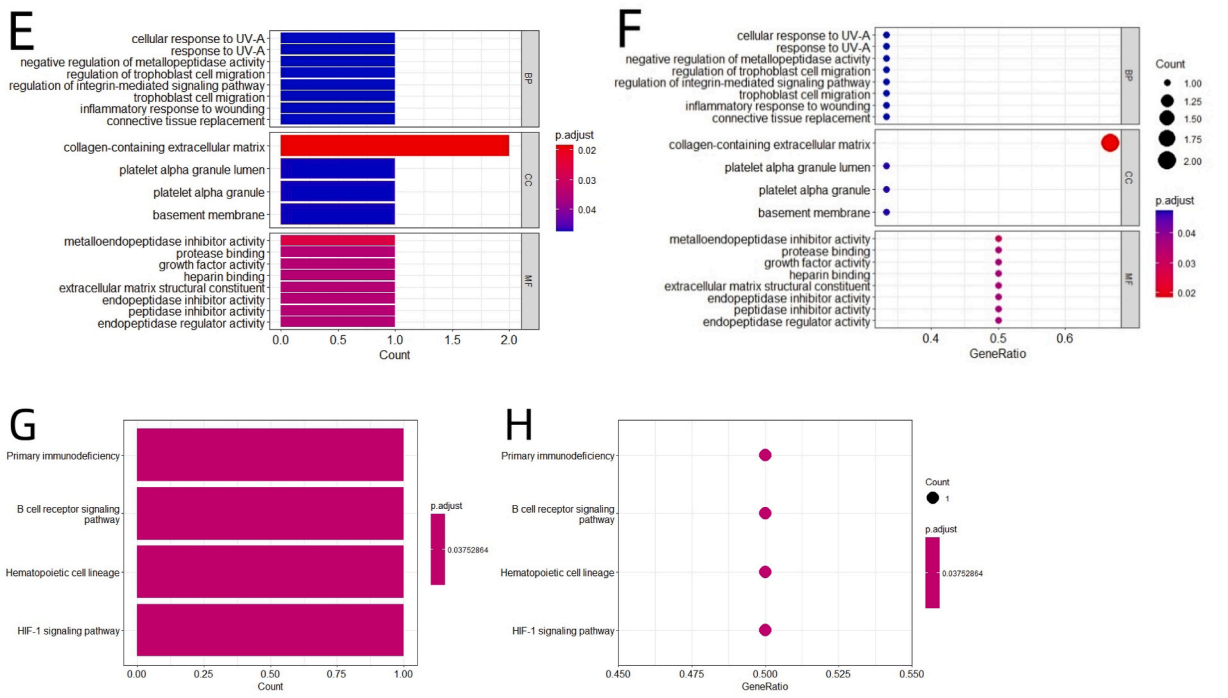

Fig. 3. (*continued*).

Table 6
GSEA results of THBS2, TIMP1, POSTN and CD19.

Hub gene	Common involved gene sets in IPF and RA-UIP through GSEA
THBS2	*Adherens junction; AGE-RAGE signaling pathway in diabetic complications; Arrhythmogenic right ventricular cardiomyopathy; Bacterial invasion of epithelial cells; ECM-receptor interaction; Ferroptosis; Focal adhesion; Influenza A; Leukocyte transendothelial migration; Mineral absorption; Necroptosis;Yersinia infection.*
TIMP1	*Adherens junction; Apoptosis; Arrhythmogenic right ventricular cardiomyopathy;Bacterial invasion of epithelial cells; Cell adhesion molecules; ECM-receptor interaction; Ferroptosis; Focal adhesion; Influenza A; Leukocyte transendothelial migration; Mineral absorption; Natural killer cell mediated cytotoxicity; Necroptosis; Phagosome; Ribosome; Small cell lung cancer; Viral myocarditis; Yersinia infection.*
POSTN	*Antigen processing and presentation; Autoimmune thyroid disease, Natural killer cell mediated cytotoxicity; Phagosome; Ribosome.*
CD19	*Antigen processing and presentation; Asthma; Autoimmune thyroid disease; Oxidative phosphorylation; Ribosome; Staphylococcus aureus infection; Systemic lupus erythematosus.*

also been reported highly associated with organ fibrosis, such as cardiac, liver, and kidney fibrosis, for it participates in the formation and repair of ECM [30–32]. Furthermore, THBS2 had previously been discovered upregulated in IPF patients, but it was rarely studied in the pathogenesis of pulmonary fibrosis [33]. Recently, a research suggested that the suppression of THBS2 resulted in the down-regulation of fibrosis-related proteins in the bleomycin-induced mice's lungs, such as α-SMA, fibronectin, and collagen I. This finding is remarkable as it highlights the potential of targeting THBS2 as a therapeutic approach for managing pulmonary fibrosis [34].

TIMP1 (metallopeptidase inhibitor 1) belongs to the TIMP gene family, encoding proteins that are natural inhibitors of matrix metalloproteinases (MMPs). How TIMP1 functions in fibrosis progression is contradictory. Given that MMPs get involved in the degradation of ECM in normal physiological processes, the overexpression of TIMP1 could cause ECM accumulation, which may promote fibrosis progression [35]. However, some MMPs have profibrotic activities during fibrosis [36], so under this premise, the inhibition of MMPs activities by TIMP1 is theoretically anti-fibrotic at some point, for a non-selective MMP inhibitor has been proven to reduce the development of bleomycin-induced pulmonary fibrosis in mice [37]. In fact, it's been observed that TIMP1 was significantly elevated in bleomycin-induced mice's lung, IPF patients' blood, sputum, and bronchoalveolar lavage fluid [38–41]. That may be because TIMP1 influences fibroblast activities such as proliferation and activation via signal transduction pathways besides being known as a MMPs' inhibitor [42]. On the whole, the role of TIMP1 in fibrosis progression is a subject of debate within the academic community, as studies yield inconclusive findings and conflicting interpretations.

POSTN (periostin) encodes a secreted extracellular matrix protein that has the ability to interact with other proteins within the extracellular matrix, so influencing the composition of the matrix in the lungs and other organs, which plays a tremendous part in collagen assembly, ECM structure, and organization. POSTN overexpression is activated by the TGF-β1 signaling pathway and connected with tumor progression and fibrosis development, for this reason, it is observed significantly upregulated in various cancers and

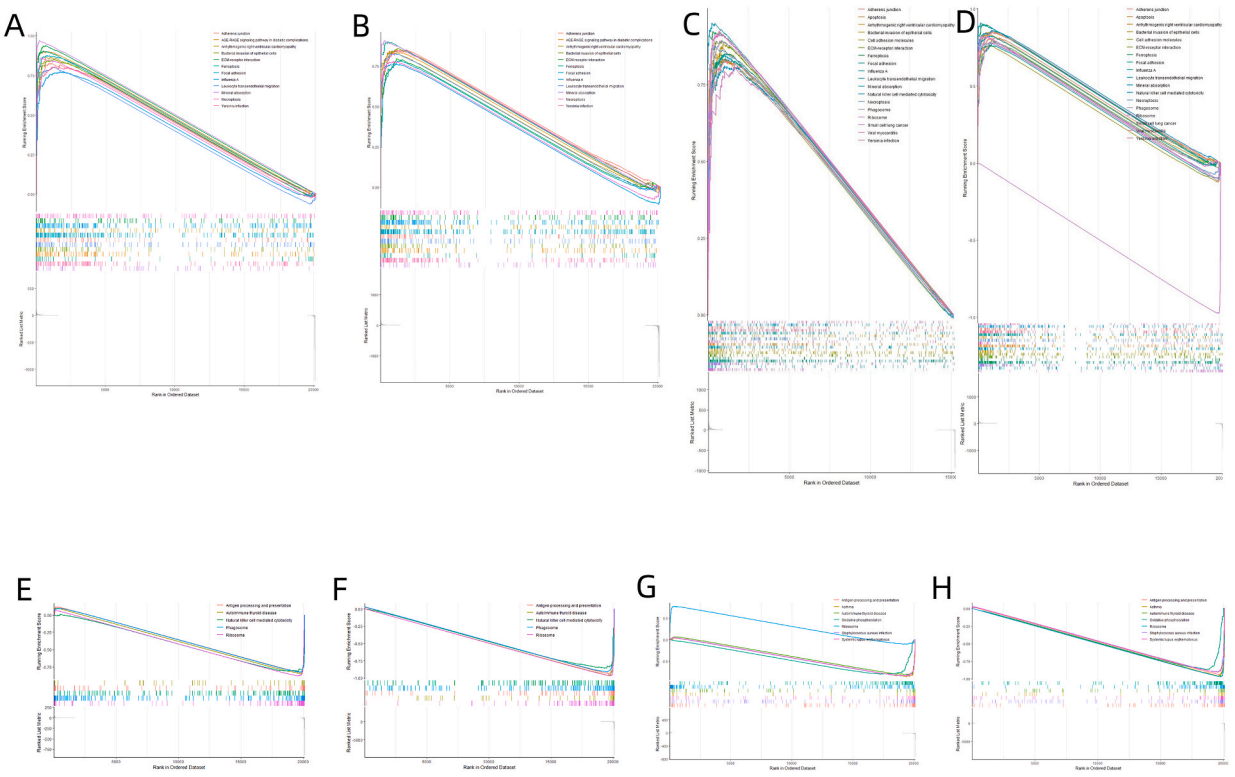

Fig. 4. GSEA of hub genes. (A).Enrichment plot of THBS2 from GSEA in IPF group. (B).Enrichment plot of THBS2 from GSEA in RA-UIP group. (C). Enrichment plot of TIMP1 from GSEA in IPF group. (D).Enrichment plot of TIMP1 from GSEA in RA-UIP group. (E).Enrichment plot of POSTN from GSEA in IPF group. (F).Enrichment plot of POSTN from GSEA in RA-UIP group. (G). Enrichment plot of CD19 from GSEA in IPF group. (H). Enrichment plot of CD19 from GSEA in RA-UIP group.

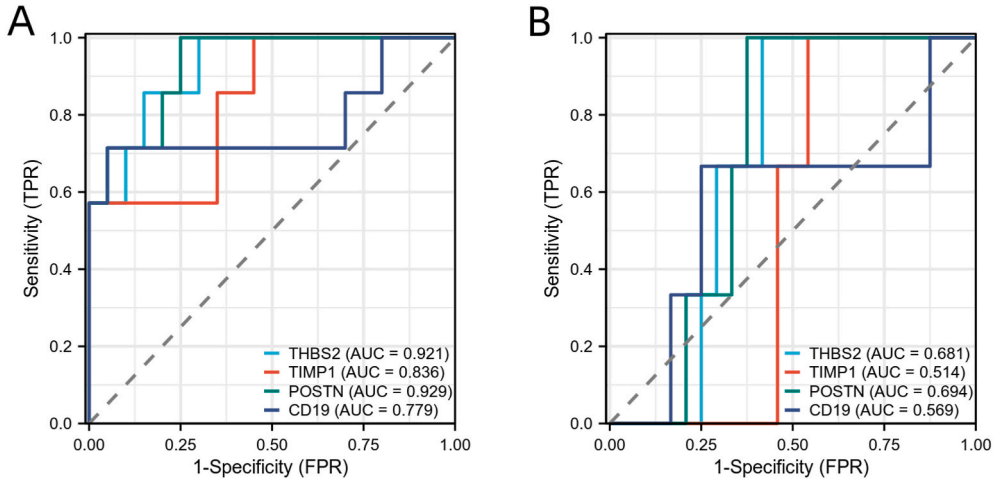

Fig. 5. Diagnostic evaluation of four core genes. (A).ROC curve of the four hub genes in IPF. (B).ROC curve of the four hub genes in RA-UIP.

different types of fibrosis [43,44]. In recent years, it has been regarded as a useful predictor of clinical progression in IPF patients [45]. In our study, POSTN was also found highly expressed in RA-UIP patients, which indicates that POSTN may potentially exhibit similar functional roles in RA-UIP patients.

The expression of the protein encoded by CD19 is restricted to B lymphocytes. It partakes in the processes of B cell activation, B cell proliferation, B cell differentiation, and the regulation of B cell antigen receptor-induced signals [46]. Though CD19 itself hasn't been proved directly associated with pulmonary fibrosis, researchers have found that the overexpression of CD19 may indirectly contribute

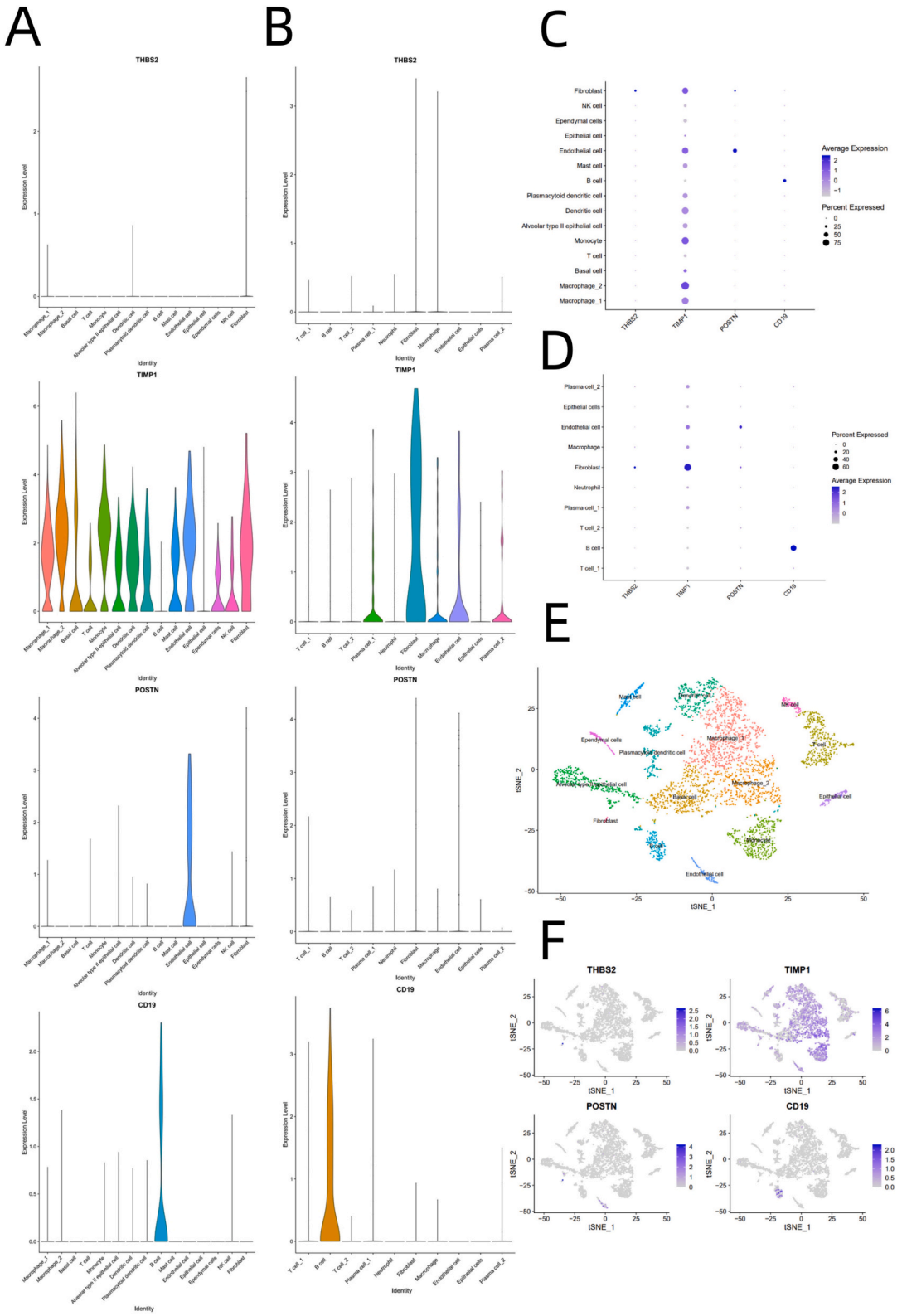

Fig. 6. scRNA-seq analyses of dataset GSE213017 and GSE180139. (A).Violinplot of expressions of hub genes in pulmonary cells of the IPF patient (GSM6568651). (B).Violinplot of expressions of hub genes in pulmonary cells of the RA-ILD patient (GSM5454350). (C). Dotplot of expressions of hub genes in pulmonary cells of the IPF patient. (D). Dotplot of expressions of hub genes in pulmonary cells of the RA-ILD patient. (E).Dimplot

visualizing cell clustering of pulmonary cells of the IPF patient. (F). Featureplot of expressions of hub genes in specific pulmonary cells of the IPF patient. (G).Dimplot visualizing cell clustering of pulmonary cells of the RA-ILD patient. (H). Featureplot of expressions of hub genes in specific pulmonary cells of the RA-ILD patient. (I).Venn diagram intersecting 110 genes between the top 200 high-expressed genes in lung fibroblasts of IPF and RA-ILD patients. (J). Dotplot of KEGG analysis of the 110 common top high-expressed genes in lung fibroblasts. (K). Dotplot of GO analysis of the 110 common top high-expressed genes in lung fibroblasts.

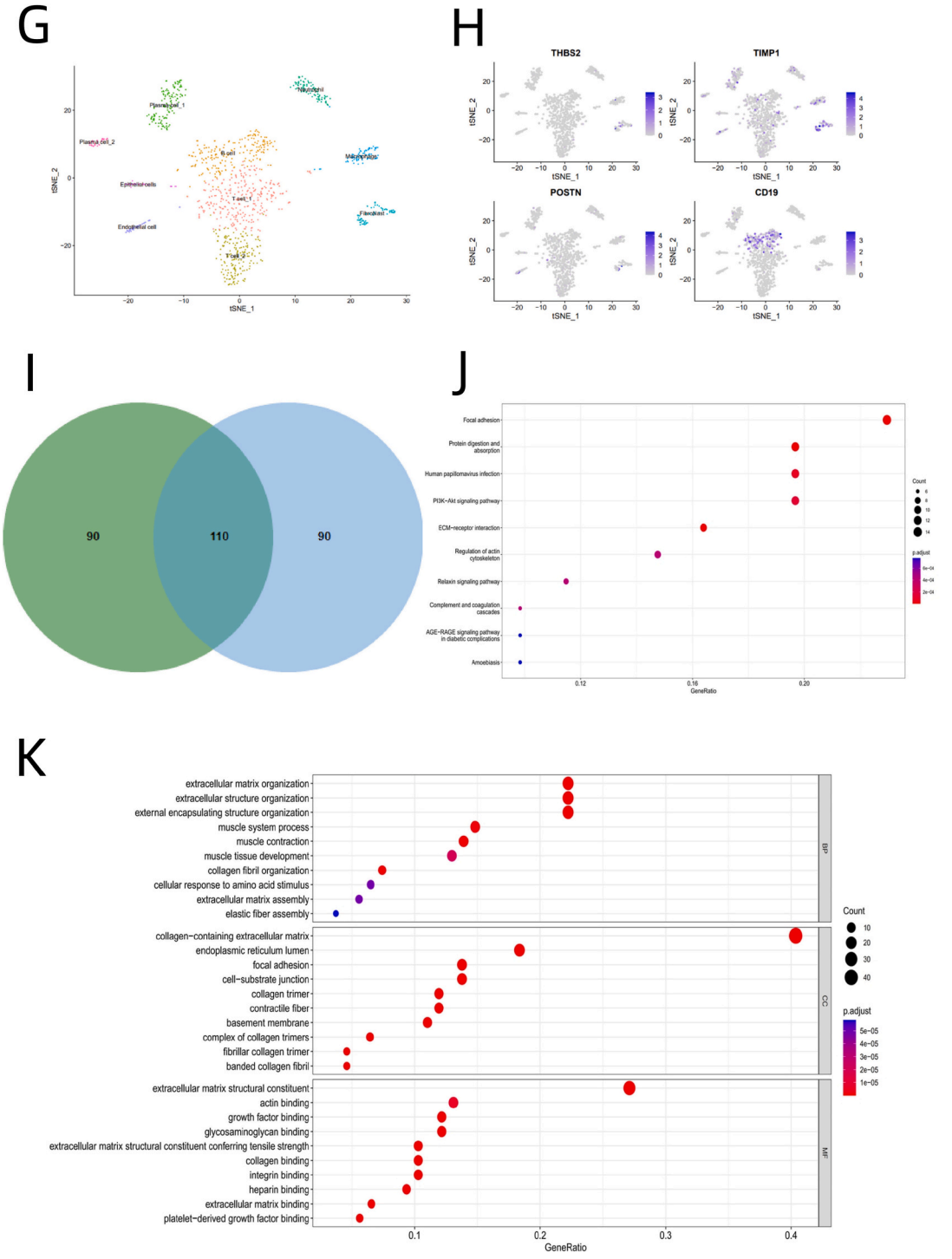

Fig. 6. (*continued*).

Table 7
The Mutual Top High Expressed Genes in Lung fibroblasts of IPF and RA-UIP Patients.

	Gene symbol
Overlapped High-expressed Genes in Fibroblasts	*AOC3; MYL9; TBX2; MFAP4; CALD1; C11orf96; FHL1; NR2F2; C1R; AEBP1; DES; RASL12; TPM2; RARRES2; LTBP1; ADIRF; TAGLN; SOD3; COL6A1; COL6A2; SMOC2; PLAC9; SERPING1; PPP1R14A; ANGPT1; DST; CAMK2N1; FRZB; BGN; IGFBP7; COL14A1; MYLK; C1S; TIMP3; TGFB1I1; EGFL6; HSPB6; FXYD1; MGP; ADAMTS1; A2M; NFIX; ID4; GPX3; COL1A2; SPARCL1; ACTA2; PLN; NBL1; CPE; LAMA4; TMEM47; PDE5A; EMILIN1; TINAGL1; PDGFRB; IGFBP5; ANTXR1; CAV1; CFH; MFGE8; PCOLCE; MXRA8; INMT; SPARC; DCN; COL5A2; NR2F1; COL4A2; CSRP2; COL18A1; COX7A1; CXCL12; SLIT3; TPM1; CNN1; SCN7A; ITGA1; FSTL1; CRIM1; FBLN1; LUM; PRELP; HOXA5; NOTCH3; MYO1B; IGFBP4; COL3A1; MYH11; LTBP4; COL1A1; KANK2; CCDC80; C7; MMP2; MCAM; CNN3; COL4A1; ELN; ITGA8; PDLIM3; SYNPO2; COL6A3; EBF1; PBX1; ENAH; THY1; CRISPLD2;FHL2; MSRB3.*

to the progression of pulmonary fibrosis through its regulation of B cell infiltration [47]. B lymphocytes, as part of the immune system, may play a role in the pathological process of lung fibrosis, for studies indicate that B cells may function in the inflammatory response and immune-mediated tissue damage processes during the course of pulmonary fibrosis [48,49]. For example, B cells are able to secrete pro-inflammatory cytokines and autoantibodies, which may cause the imbalance of tissue damage and repair, ultimately promoting the progression of pulmonary fibrosis [48]. In general, B cells may serve as a bridge for how CD19 affects the pathogenesis of IPF and RA-UIP.

GO and KEGG analyses demonstrate that the common DEGs and hub genes in IPF and RA-UIP are mainly involved in the development and organization of ECM and various collagenous structures, cellular processes and signal transduction mechanisms that influence tissue development and repair, activities of proteinases including metalloproteinases, inflammatory and immune responses, cell interactions and binding, as well as the activation of pathways related to tissue remodeling, most of which are considered to be connected with fibrosis progression [11,50–57]. On one hand, this suggests that there are shared pathological mechanisms of pulmonary fibrosis in both IPF and RA-UIP patients. On the other hand, it shows that modifying these DEGs-enriched pathways, or intervening in the biological activities of hub genes, may offer clues for the treatment of IPF and RA-UIP. Besides, it's worth mentioning that the hub genes are also enriched in biological functions that haven't been proven relevant to lung fibrosis, such as cellular response to ultraviolet, indicating that the hub genes participate in a multitude of complex physiological processes.

GSEA analysis indicated that the core genes may serve multiple biological processes in IPF and RA-UIP, such as cell-ECM interaction, cell adhesion, programmed cell death, and immunoregulation. It's also revealed in GSEA analysis that the hub genes are likely to get involved in many diseases like small cell lung cancer, virus infection, bacterial infection, diabetes, asthma, and autoimmune diseases, which may have associations with the occurrence and development of UIP, for some of these diseases have been reported relevant to lung fibrosis [58–63]. It is remarkable that the activation of pathway 'Ribosome' is closely interacted with higher expression of TIMP1 and CD19 in the IPF group (Fig. 4C and . G), but with lower expression of them in the RA-UIP group (Fig. 4D and . H). It may prompt that the functions of TIMP1 and CD19 slightly differ between the two diseases. Nevertheless, due to the fact that the results of GSEA analysis haven't been proven by experiments, further studies are required.

scRNA-seq analysis provides detailed and targeted information on hub gene expression differences that may be critical to understanding the pathogenesis of pulmonary fibrosis in both IPF and RA-UIP patients. As the abnormal activation and excessive proliferation of fibroblasts promote the progression of lung fibrosis, the high expression of THBS2, TIMP1, and POSTN in fibroblasts of IPF and RA-ILD patients may suggest their roles in the fibrotic processes. Taking the enrichment analysis results of common top high-expressed genes in lung fibroblasts as a reference (Fig. 6J–K), and in conjunction with the biological functions of THBS2, TIMP1, and POSTN previously mentioned, we hypothesize that these 3 key genes may also be involved in fibroblast-associated pathways such as muscle tissue development, cell adhesion, and ECM organization. Consequently, the dysfunction of these genes and other highly expressed genes in fibroblasts could potentially contribute to the development of pulmonary fibrosis in IPF and RA-UIP patients. Among these, the specific upregulation of THBS2 in lung fibroblasts may point to a potential target for therapeutic intervention. Additionally, the exclusively high expression of CD19 in B cells suggests possible immunological factors for these diseases, particularly since B cells are involved in the autoimmune response and CD19 is a marker for B cell activation [47]. As a result, CD19 has been under study as a promising B cell target for fibrotic pulmonary diseases. Studies have found that treatments targeting CD19 can reduce the release of inflammatory mediators and inhibit the activities of B cells, thereby alleviating lung interstitial fibrotic lesions, improving lung function, and relieving symptoms [47,64,65]. However, the specific treatment effects and efficacy still require further research and clinical trials for verification.

According to bioinformatics analysis results, the expression levels of the four core genes were subsequently verified by qRT-PCR using clinical and cellular specimens, as well as by IHC using experimental animal samples. The qRT-PCR and IHC results verified that the expression levels of the core genes were mostly in accordance with the outcomes of the bioinformatics analyses. Yet, out of anticipation, the mRNA expression levels of TIMP1 demonstrated no significant difference either between the IPF patients and controls or between the RA-UIP patients and controls. This result may be restricted by the number of samples and the type of samples. What's more, the mRNA levels of one gene are affected by many factors, such as states, individuals, and measurement techniques, and don't always predict its protein levels [66]. Hence, mRNA levels should not be interpreted as the final output of gene expression.

The reliability of the key genes was also validated through external datasets. Interestingly, THBS2, TIMP1, POSTN, and CD19 were observed to be upregulated in the cohort of general RA patients, which prompts that the 4 hub genes may get involved in mechanisms of RA, not limited to the RA-UIP subtype. In fact, some of the key genes have been under study as diagnostic biomarkers and therapeutic targets for RA patients [67–69].

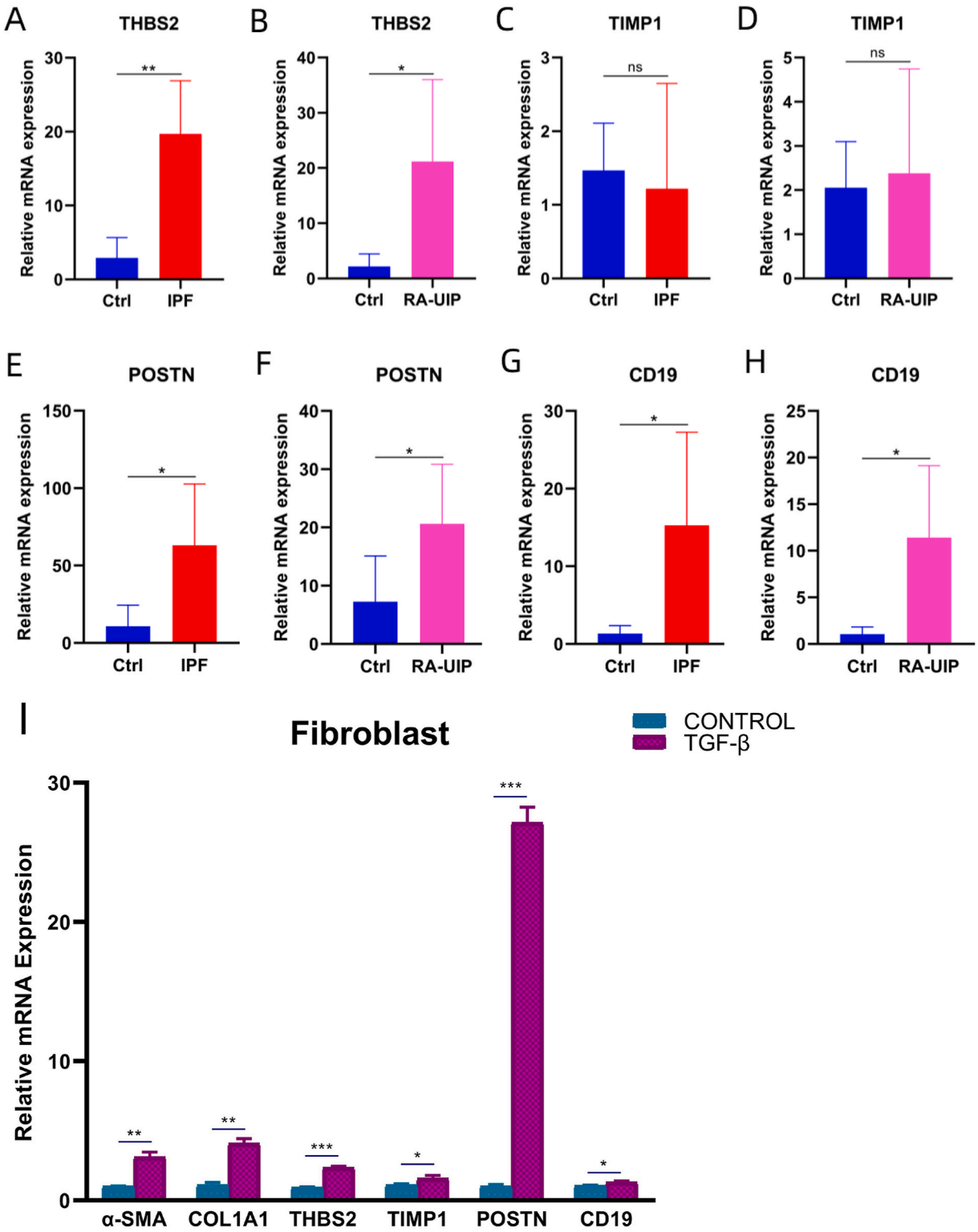

Fig. 7. Verification of Hub Genes (A).Barplot of mRNA expression levels of THBS2 between IPF and control group. (B).Barplot of mRNA expression levels of THBS2 between RA-UIP and control group. (C).Barplot of mRNA expression levels of TIMP1 between IPF and control group. (D).Barplot of mRNA expression levels of TIMP1 between RA-UIP and control group. (E).Barplot of mRNA expression levels of POSTN between IPF and control group. (F).Barplot of mRNA expression levels of POSTN between RA-UIP and control group. (G).Barplot of mRNA expression levels of CD19 between the IPF and control group. (H).Barplot of mRNA expression levels of CD19 between RA-UIP and control group. (I).Barplot of mRNA expression levels

of α-SMA, COL1A1, and hub genes between TGF-β1-stimulated fibroblast group and control group. (J).Images of H&E staining (H&Ex200) and immunohistochemical staining (DABx200) of bleomycin-induced mouse group and control group. (K).Scatter plots of positive immunostained area proportions of α-SMA, COL1A1, and hub genes between bleomycin-induced mouse group and control group. (L).Boxplot of mRNA expression levels of hub genes between IPF and control group on dataset GSE150910. (M).Boxplot of mRNA expression levels of hub genes between RA and control group on dataset GSE89408.
Notes:*p less than 0.05, **p less than 0.01, ***p less than 0.001, ****p less than 0.0001, and ns, no significance.

There are some flaws in this study. Firstly, the bioinformatics findings were derived from the lung tissues of patients and controls, but we conducted experimental validation on the blood samples of the participants. Secondly, the number of clinical and experimental animal samples is restricted, and larger subsets are required to confirm our conclusions. Moreover, the in vitro and animal models may not be able to precisely simulate the pathological state of patients with RA-UIP. However, there are currently no widely-acknowledged models for RA-UIP in the academic community [70]. Last but not least, it's a pity that we didn't perform experiments to investigate the protein expression levels of the core genes in patient samples because of the limitations of our experimental designs and expenses. Generally speaking, more experiments are supposed to be performed for further verification in the future.

5. Conclusions

The research identifies THBS2, TIMP1, POSTN, and CD19 as mutual key biomarkers in IPF and RA-UIP with integrated bioinformatics methods. The validation of qRT-PCR, IHC, and external datasets demonstrates that the relative expression levels of the hub genes are generally consistent with the findings obtained from the bioinformatics methods. Enrichment analyses show that the selected genes may be associated with the onset of IPF and RA-UIP by regulating pulmonary fibrosis progression. As common biomarkers, THBS2, TIMP1, POSTN, and CD19 may exert essential functions in the development of IPF and RA-UIP and be underlying targets for the treatment. Future research directions could focus on the interventions targeting these hub genes and related pathways.

Ethics statement

This research and involved experimental procedures were approved by the Research Ethics Committee of Guangdong Provincial People's Hospital (Guangdong Academy of Medical Sciences). The ethics approval number was No.GDREC20160679H (R1). Written informed consent was obtained from all participants in the study.

Data availability statement

The datasets analyzed during the current study are available in the GEO database (https://www.ncbi.nlm.nih.gov/geo/). These accession numbers for the datasets are GSE199152, GSE213017, GSE180139, GSE150910, and GSE89408. Any additional information required to reanalyze the data are available from the corresponding author on request.

CRediT authorship contribution statement

Liangyu Chen: Writing – original draft, Visualization, Validation, Software, Resources, Methodology, Investigation, Formal analysis, Data curation, Conceptualization. **Haobo Lin:** Writing – review & editing, Supervision, Project administration, Methodology, Conceptualization. **Linmang Qin:** Validation, Software, Resources, Investigation, Data curation. **Guangfeng Zhang:** Validation, Supervision, Resources, Methodology. **Donghui Huang:** Writing – review & editing, Supervision. **Peisheng Chen:** Writing – review & editing, Resources, Formal analysis. **Xiao Zhang:** Writing – review & editing, Supervision, Resources, Project administration, Methodology, Conceptualization.

Declaration of generative AI and AI-assisted technologies in the writing process

During the preparation of this work, the authors used ChatGPT in order to improve language and readability. After using this tool, the authors reviewed and edited the content as needed and take full responsibility for the content of the publication.

Declaration of competing interest

The authors declare the following financial interests/personal relationships which may be considered as potential competing interests:Xiao Zhang reports financial support was provided by National Natural Science Foundation of China. Haobo Lin reports financial support was provided by Natural Science Foundation of Guangdong Province. Haobo Lin reports financial support was provided by Bureau of Science and Technology of Guangzhou Municipality. Haobo Lin reports financial support was provided by Medical Scientific Research Foundation of Guangdong Province. Donghui Huang reports financial support was provided by Zhuhai City Health Bureau. Donghui Huang reports financial support was provided by Zhuhai Science and Technology Innovation Bureau. If there are other authors, they declare that they have no known competing financial interests or personal relationships that could have appeared to influence the work reported in this paper.

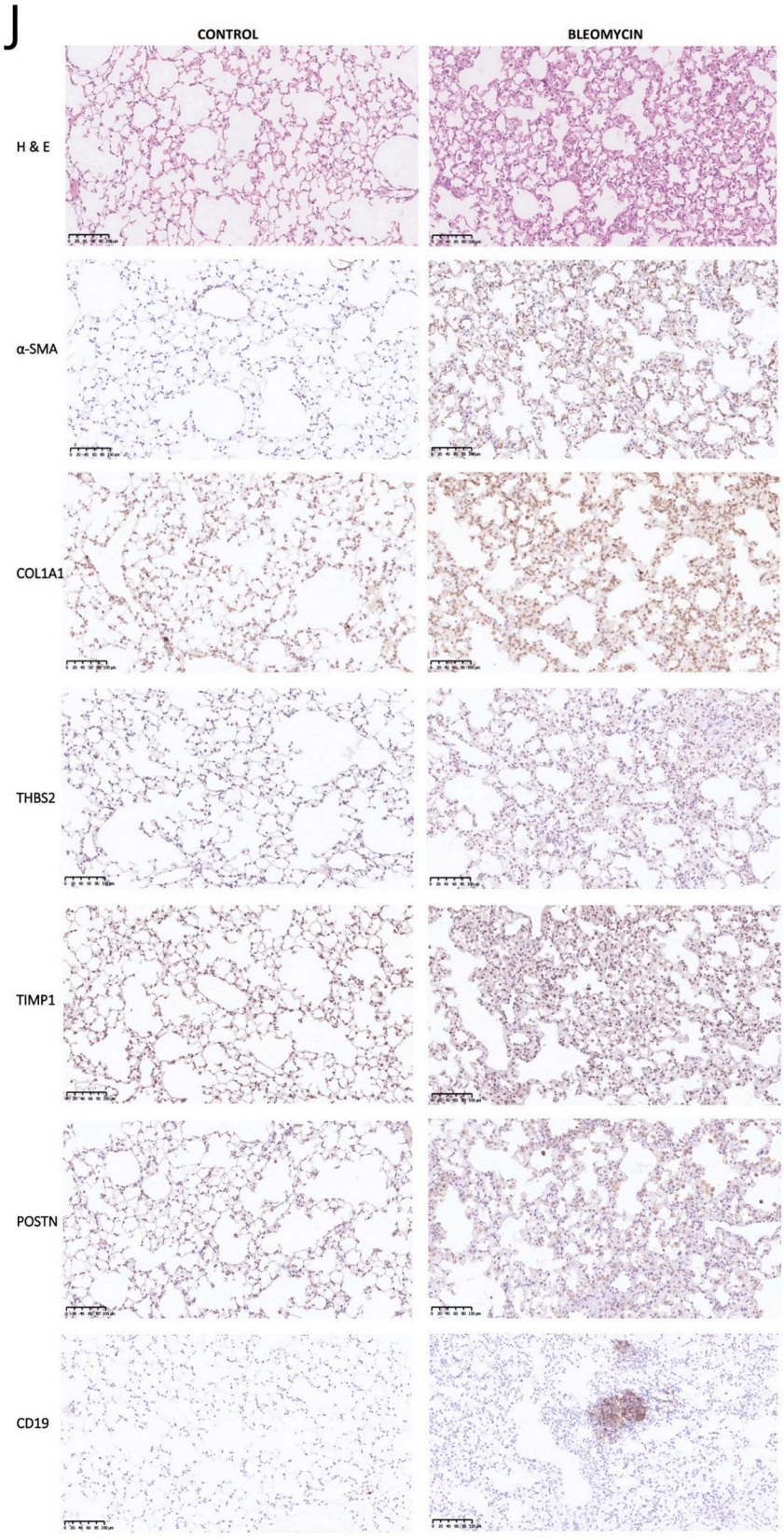
J
CONTROL
BLEOMYCIN
H & E
α-SMA
COL1A1
THBS2
TIMP1
POSTN
CD19

Fig. 7. (*continued*).

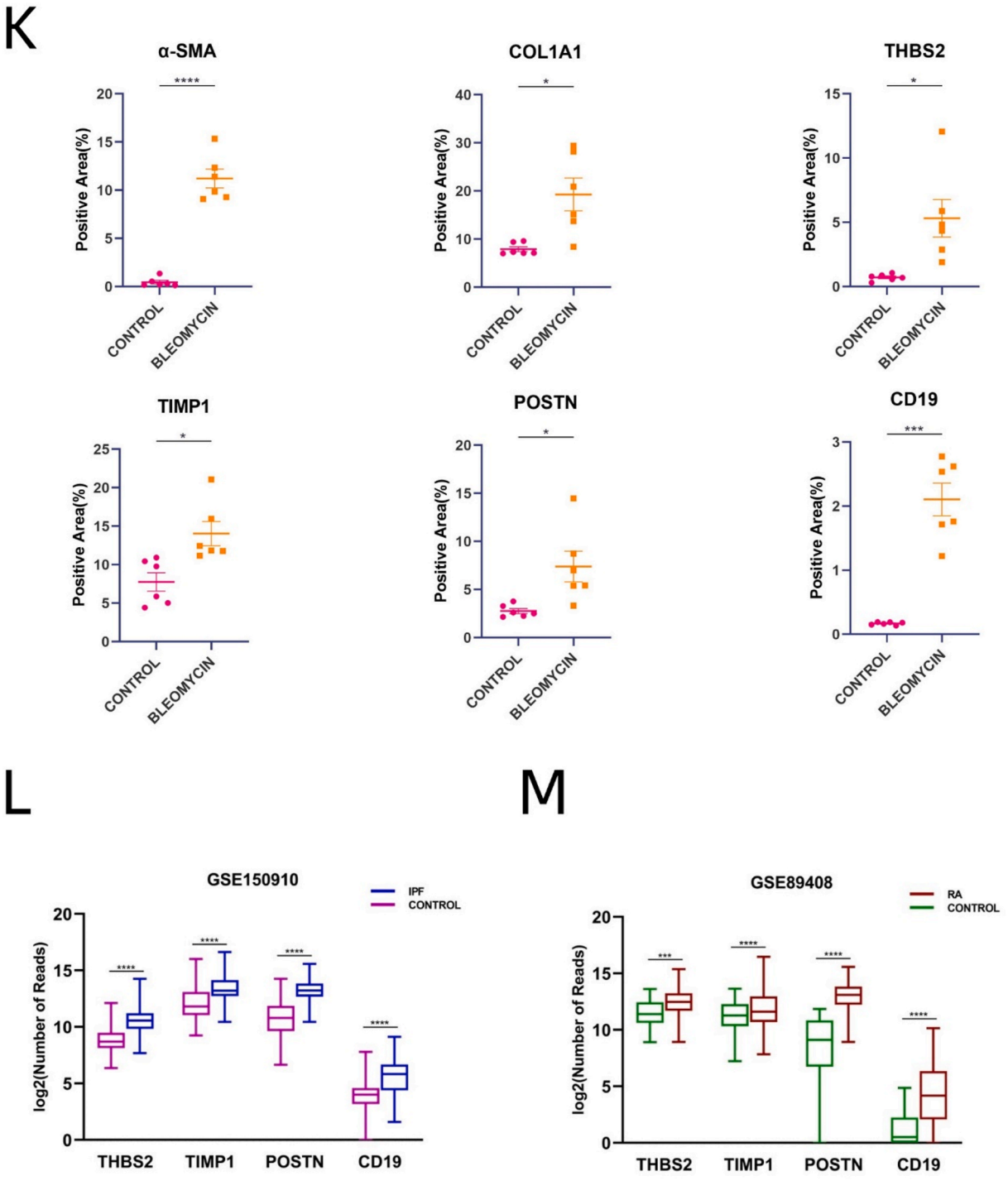

Fig. 7. (*continued*).

Acknowledgments

This work was supported by the Natural Science Foundation of Guangdong Province (2019A1515010927); the National Natural Science Foundation of China (81771734 & 82271822); the Science and Technology Program of Guangzhou (202102021181 & 202201011346); the Medical Scientiffc Research Foundation of Guangdong Province (A2019139); Zhuhai City Health Bureau

(2220009000235); and Zhuhai Science and Technology Innovation Bureau (2320004000290). The authors express their gratitude to Dr. Zuogeng Hong, Dr. Rujin Ju, Dr. Ke Yuan, Dr. Wei Deng, and Dr. Chuanfan Xu for their professional opinions and advices on the article.

Appendix A. Supplementary data

Supplementary data to this article can be found online at https://doi.org/10.1016/j.heliyon.2024.e28088.

References

[1] G. Sgalla, A. Biffi, L. Richeldi, Idiopathic pulmonary fibrosis: diagnosis, epidemiology and natural history, Respirology 21 (3) (2016) 427–437, https://doi.org/10.1111/resp.12683.
[2] L. Cavagna, S. Monti, V. Grosso, et al., The multifaceted aspects of interstitial lung disease in rheumatoid arthritis, BioMed Res. Int. 2013 (2013) 759760, https://doi.org/10.1155/2013/759760.
[3] S. Matson, J. Lee, O. Eickelberg, Two sides of the same coin? A review of the similarities and differences between idiopathic pulmonary fibrosis and rheumatoid arthritis-associated interstitial lung disease, Eur. Respir. J. 57 (5) (2021) 2002533, https://doi.org/10.1183/13993003.02533-2020. Published 2021 May 13.
[4] P.A. Juge, B. Crestani, P. Dieudé, Recent advances in rheumatoid arthritis-associated interstitial lung disease, Curr. Opin. Pulm. Med. 26 (5) (2020) 477–486, https://doi.org/10.1097/MCP.0000000000000710.
[5] S. Wang, M. Liu, X. Li, et al., Canonical and noncanonical regulatory roles for JAK2 in the pathogenesis of rheumatoid arthritis-associated interstitial lung disease and idiopathic pulmonary fibrosis, Faseb. J. 36 (6) (2022) e22336, https://doi.org/10.1096/fj.202101436R.
[6] A. Löfdahl, G. Tornling, J. Wigén, et al., Pathological insight into 5-HT2B receptor activation in fibrosing interstitial lung diseases, Int. J. Mol. Sci. 22 (1) (2020) 225, https://doi.org/10.3390/ijms22010225. Published 2020 Dec 28.
[7] K.D. Samara, A. Trachalaki, E. Tsitoura, et al., Upregulation of citrullination pathway: from autoimmune to idiopathic lung fibrosis, Respir. Res. 18 (1) (2017) 218, https://doi.org/10.1186/s12931-017-0692-9. Published 2017 Dec 29.
[8] JP 3rd Lynch, R. Saggar, S.S. Weigt, et al., Usual interstitial pneumonia, Semin. Respir. Crit. Care Med. 27 (6) (2006) 634–651, https://doi.org/10.1055/s-2006-957335.
[9] E.S. White, M.H. Lazar, V.J. Thannickal, Pathogenetic mechanisms in usual interstitial pneumonia/idiopathic pulmonary fibrosis, J. Pathol. 201 (3) (2003 Nov) 343–354, https://doi.org/10.1002/path.1446. PMID: 14595745; PMCID: PMC2810622.
[10] H. Ma, S. Liu, S. Li, Y. Xia, Targeting growth factor and cytokine pathways to treat idiopathic pulmonary fibrosis, Front. Pharmacol. 13 (2022 Jun 3) 918771, https://doi.org/10.3389/fphar.2022.918771. PMID: 35721111; PMCID: PMC9204157.
[11] L. Qin, H. Lin, F. Zhu, et al., CD4+LAG3+T cells are decreased in SSc-ILD and affect fibroblast mesenchymal transition by TGF-β3, iScience 26 (12) (2023) 108225, https://doi.org/10.1016/j.isci.2023.108225. Published 2023 Oct 17.
[12] W. Yang, L. Pan, Y. Cheng, et al., Nintedanib alleviates pulmonary fibrosis in vitro and in vivo by inhibiting the FAK/ERK/S100A4 signalling pathway, Int. Immunopharm. 113 (Pt A) (2022) 109409, https://doi.org/10.1016/j.intimp.2022.109409.
[13] V. Della Latta, A. Cecchettini, Ry S. Del, et al., Bleomycin in the setting of lung fibrosis induction: from biological mechanisms to counteractions, Pharmacol. Res. 97 (2015) 122–130, https://doi.org/10.1016/j.phrs.2015.04.012.
[14] P. Kolb, C. Upagupta, M. Vierhout, et al., The importance of interventional timing in the bleomycin model of pulmonary fibrosis, Eur. Respir. J. 55 (6) (2020) 1901105, https://doi.org/10.1183/13993003.01105-2019. Published 2020 Jun 11.
[15] M.I. Love, W. Huber, S. Anders, Moderated estimation of fold change and dispersion for RNA-seq data with DESeq2, Genome Biol. 15 (12) (2014) 550, https://doi.org/10.1186/s13059-014-0550-8.
[16] M.E. Smoot, K. Ono, J. Ruscheinski, et al., Cytoscape 2.8: new features for data integration and network visualization, Bioinformatics 27 (3) (2011 Feb 1) 431–432, https://doi.org/10.1093/bioinformatics/btq675. Epub 2010 Dec 12. PMID: 21149340; PMCID: PMC3031041.
[17] Q. Gao, L. Fan, Y. Chen, et al., Identification of the hub and prognostic genes in liver hepatocellular carcinoma via bioinformatics analysis, Front. Mol. Biosci. 9 (2022 Sep 29) 1000847, https://doi.org/10.3389/fmolb.2022.1000847. PMID: 36250027; PMCID: PMC9557295.
[18] M. Gao, W. Kong, Z. Huang, et al., Identification of key genes related to lung squamous cell carcinoma using bioinformatics analysis, Int. J. Mol. Sci. 21 (8) (2020 Apr 23) 2994, https://doi.org/10.3390/ijms21082994. PMID: 32340320; PMCID: PMC7215920.
[19] M. Ashburner, C.A. Ball, J.A. Blake, et al., Gene ontology: tool for the unification of biology. The Gene Ontology Consortium, Nat. Genet. 25 (1) (2000) 25–29, https://doi.org/10.1038/75556.
[20] M. Kanehisa, S. Goto, KEGG: kyoto encyclopedia of genes and genomes, Nucleic Acids Res. 28 (1) (2000) 27–30, https://doi.org/10.1093/nar/28.1.27.
[21] A. Subramanian, P. Tamayo, V.K. Mootha, et al., Gene set enrichment analysis: a knowledge-based approach for interpreting genome-wide expression profiles, Proc. Natl. Acad. Sci. U.S.A. 102 (43) (2005) 15545–15550, https://doi.org/10.1073/pnas.0506580102.
[22] X. Robin, N. Turck, A. Hainard, et al., pROC: an open-source package for R and S+ to analyze and compare ROC curves, BMC Bioinf. 12 (2011 Mar 17) 77, https://doi.org/10.1186/1471-2105-12-77. PMID: 21414208; PMCID: PMC3068975.
[23] Q. Huang, Y. Liu, Y. Du, et al., Evaluation of cell type annotation R packages on single-cell RNA-seq data, Dev. Reprod. Biol. 19 (2) (2021) 267–281, https://doi.org/10.1016/j.gpb.2020.07.004.
[24] O. Franzén, L.M. Gan, J.L.M. Björkegren, PanglaoDB: a web server for exploration of mouse and human single-cell RNA sequencing data, Database 2019 (2019 Jan 1) baz046, https://doi.org/10.1093/database/baz046. PMID: 30951143; PMCID: PMC6450036.
[25] X. Zhang, Y. Lan, J. Xu, et al., CellMarker: a manually curated resource of cell markers in human and mouse, Nucleic Acids Res. 47 (D1) (2019 Jan 8) D721–D728, https://doi.org/10.1093/nar/gky900. PMID: 30289549; PMCID: PMC6323899.
[26] G. Raghu, M. Remy-Jardin, L. Richeldi, et al., Idiopathic pulmonary fibrosis (an update) and progressive pulmonary fibrosis in adults: an official ATS/ERS/JRS/ALAT clinical practice guideline, Am. J. Respir. Crit. Care Med. 205 (9) (2022 May 1) e18–e47, https://doi.org/10.1164/rccm.202202-0399ST.
[27] D. Aletaha, T. Neogi, A.J. Silman, et al., 2010 rheumatoid arthritis classification criteria: an American College of Rheumatology/European League against Rheumatism collaborative initiative [published correction appears in Ann Rheum Dis. 2010 Oct;69(10):1892], Ann. Rheum. Dis. 69 (9) (2010) 1580–1588, https://doi.org/10.1136/ard.2010.138461.
[28] J. Shu, G.E. Dolman, J. Duan, et al., Statistical colour models: an automated digital image analysis method for quantification of histological biomarkers, Biomed. Eng. Online 15 (2016 Apr 27) 46, https://doi.org/10.1186/s12938-016-0161-6. PMID: 27121383; PMCID: PMC4848853.
[29] L. Wang, L. Zhao, Y. Wang, Circular RNA circ_0020123 promotes non-small cell lung cancer progression by sponging miR-590-5p to regulate THBS2, Cancer Cell Int. 20 (2020) 387, https://doi.org/10.1186/s12935-020-01444-z. Published 2020 Aug 11.
[30] Y. Lou, G.Y. Tian, Y. Song, et al., Characterization of transcriptional modules related to fibrosing-NAFLD progression, Sci. Rep. 7 (1) (2017) 4748, https://doi.org/10.1038/s41598-017-05044-2. Published 2017 Jul 6.
[31] C.H. Hsu, I.F. Liu, H.F. Kuo, et al., miR-29a-3p/THBS2 Axis regulates PAH-induced cardiac fibrosis, Int. J. Mol. Sci. 22 (19) (2021) 10574, https://doi.org/10.3390/ijms221910574. Published 2021 Sep. 30.

[32] M. Jerala, N. Hauptman, N. Kojc, N. Zidar, Expression of fibrosis-related genes in liver and kidney fibrosis in comparison to inflammatory bowel diseases, Cells 11 (3) (2022) 314, https://doi.org/10.3390/cells11030314. Published 2022 Jan 18.

[33] Y. Cui, J. Ji, J. Hou, Y. Tan, X. Han, Identification of key candidate genes involved in the progression of idiopathic pulmonary fibrosis, Molecules 26 (4) (2021) 1123, https://doi.org/10.3390/molecules26041123. Published 2021 Feb 20.

[34] Q. Liu, Y. Bi, S. Song, et al., Exosomal miR-17-5p from human embryonic stem cells prevents pulmonary fibrosis by targeting thrombospondin-2, Stem Cell Res. Ther. 14 (1) (2023 Sep 4) 234, https://doi.org/10.1186/s13287-023-03449-7.

[35] S. Robert, T. Gicquel, T. Victoni, et al., Involvement of matrix metalloproteinases (MMPs) and inflammasome pathway in molecular mechanisms of fibrosis, Biosci. Rep. 36 (4) (2016 Jul 15) e00360, https://doi.org/10.1042/BSR20160107.

[36] M. Giannandrea, W.C. Parks, Diverse functions of matrix metalloproteinases during fibrosis, Dis Model Mech 7 (2) (2014) 193–203, https://doi.org/10.1242/dmm.012062.

[37] M. Corbel, S. Caulet-Maugendre, N. Germain, S. Molet, V. Lagente, E. Boichot, Inhibition of bleomycin-induced pulmonary fibrosis in mice by the matrix metalloproteinase inhibitor batimastat, J. Pathol. 193 (4) (2001) 538–545, https://doi.org/10.1002/path.826.

[38] H. Ovet, F. Oztay, The copper chelator tetrathiomolybdate regressed bleomycin-induced pulmonary fibrosis in mice, by reducing lysyl oxidase expressions, Biol. Trace Elem. Res. 162 (1–3) (2014) 189–199, https://doi.org/10.1007/s12011-014-0142-1.

[39] J.L. Todd, R. Vinisko, Y. Liu, et al., Circulating matrix metalloproteinases and tissue metalloproteinase inhibitors in patients with idiopathic pulmonary fibrosis in the multicenter IPF-PRO Registry cohort, BMC Pulm. Med. 20 (1) (2020 Mar 14) 64, https://doi.org/10.1186/s12890-020-1103-4.

[40] K.M. Beeh, J. Beier, O. Kornmann, R. Buhl, Sputum matrix metalloproteinase-9, tissue inhibitor of metalloprotinease-1, and their molar ratio in patients with chronic obstructive pulmonary disease, idiopathic pulmonary fibrosis and healthy subjects, Respir. Med. 97 (6) (2003) 634–639, https://doi.org/10.1053/rmed.2003.1493.

[41] S. Willems, S.E. Verleden, B.M. Vanaudenaerde, et al., Multiplex protein profiling of bronchoalveolar lavage in idiopathic pulmonary fibrosis and hypersensitivity pneumonitis, Ann. Thorac. Med. 8 (1) (2013 Jan) 38–45, https://doi.org/10.4103/1817-1737.105718.

[42] J. Dong, Q. Ma, TIMP1 promotes multi-walled carbon nanotube-induced lung fibrosis by stimulating fibroblast activation and proliferation, Nanotoxicology 11 (1) (2017 Feb) 41–51, https://doi.org/10.1080/17435390.2016.1262919.

[43] H. Yue, W. Li, R. Chen, J. Wang, X. Lu, J. Li, Stromal POSTN induced by TGF-β1 facilitates the migration and invasion of ovarian cancer, Gynecol. Oncol. 160 (2) (2021) 530–538, https://doi.org/10.1016/j.ygyno.2020.11.026.

[44] M. Kreus, S. Lehtonen, S. Skarp, R. Kaarteenaho, Extracellular matrix proteins produced by stromal cells in idiopathic pulmonary fibrosis and lung adenocarcinoma, PLoS One 16 (4) (2021) e0250109, https://doi.org/10.1371/journal.pone.0250109. Published 2021 Apr 27.

[45] P.K. Naik, P.D. Bozyk, J.K. Bentley, et al., Periostin promotes fibrosis and predicts progression in patients with idiopathic pulmonary fibrosis, Am. J. Physiol. Lung Cell Mol. Physiol. 303 (12) (2012 Dec 15) L1046–L1056, https://doi.org/10.1152/ajplung.00139.2012. Epub 2012 Oct 5.

[46] P. Engel, L.J. Zhou, D.C. Ord, S. Sato, B. Koller, T.F. Tedder, Abnormal B lymphocyte development, activation, and differentiation in mice that lack or overexpress the CD19 signal transduction molecule, Immunity 3 (1) (1995) 39–50, https://doi.org/10.1016/1074-7613(95)90157-4.

[47] K. Komura, K. Yanaba, M. Horikawa, et al., CD19 regulates the development of bleomycin-induced pulmonary fibrosis in a mouse model, Arthritis Rheum. 58 (11) (2008) 3574–3584, https://doi.org/10.1002/art.23995.

[48] N.W. Todd, I.G. Luzina, S.P. Atamas, Molecular and cellular mechanisms of pulmonary fibrosis, Fibrogenesis Tissue Repair 5 (1) (2012 Jul 23) 11, https://doi.org/10.1186/1755-1536-5-11. PMID: 22824096; PMCID: PMC3443459.

[49] J. Xue, D.J. Kass, J. Bon, et al., Plasma B lymphocyte stimulator and B cell differentiation in idiopathic pulmonary fibrosis patients, J. Immunol. 191 (5) (2013 Sep 1) 2089–2095, https://doi.org/10.4049/jimmunol.1203476. Epub 2013 Jul 19. PMID: 23872052; PMCID: PMC3804013.

[50] G. Liu, A.M. Philp, T. Corte, et al., Therapeutic targets in lung tissue remodelling and fibrosis, Pharmacol. Ther. 225 (2021) 107839, https://doi.org/10.1016/j.pharmthera.2021.107839.

[51] V.J. Craig, L. Zhang, J.S. Hagood, et al., Matrix metalloproteinases as therapeutic targets for idiopathic pulmonary fibrosis, Am. J. Respir. Cell Mol. Biol. 53 (5) (2015) 585–600, https://doi.org/10.1165/rcmb.2015-0020TR.

[52] P. Heukels, C.C. Moor, J.H. von der Thüsen, et al., Inflammation and immunity in IPF pathogenesis and treatment, Respir. Med. 147 (2019) 79–91, https://doi.org/10.1016/j.rmed.2018.12.015.

[53] B.J. Moss, S.W. Ryter, I.O. Rosas, Pathogenic mechanisms underlying idiopathic pulmonary fibrosis, Annu. Rev. Pathol. 17 (2022) 515–546, https://doi.org/10.1146/annurev-pathol-042320-030240.

[54] M. Zhao, L. Wang, M. Wang, et al., Targeting fibrosis, mechanisms and cilinical trials, Signal Transduct. Targeted Ther. 7 (1) (2022) 206, https://doi.org/10.1038/s41392-022-01070-3. Published 2022 Jun 30.

[55] O. Burgy, M. Königshoff, The WNT signaling pathways in wound healing and fibrosis, Matrix Biol. 68–69 (2018) 67–80, https://doi.org/10.1016/j.matbio.2018.03.017.

[56] J. Wang, K. Hu, X. Cai, et al., Targeting PI3K/AKT signaling for treatment of idiopathic pulmonary fibrosis, Acta Pharm. Sin. B 12 (1) (2022) 18–32, https://doi.org/10.1016/j.apsb.2021.07.023.

[57] F. Qian, M. He, W. Duan, et al., Cross regulation between hypoxia-inducible transcription factor-1α (HIF-1α) and transforming growth factor (TGF)-ß1 mediates nickel oxide nanoparticles (NiONPs)-induced pulmonary fibrosis, Am J Transl Res 7 (11) (2015 Nov 15) 2364–2378. PMID: 26807184; PMCID: PMC4697716.

[58] X. Zhang, W. Li, C. Li, J. Zhang, Z. Su, Chemotherapy in idiopathic pulmonary fibrosis and small-cell lung cancer with poor lung function, BMC Pulm. Med. 21 (1) (2021) 122, https://doi.org/10.1186/s12890-021-01489-4. Published 2021 Apr 15.

[59] W.J. Huang, X.X. Tang, Virus infection induced pulmonary fibrosis, J. Transl. Med. 19 (1) (2021) 496, https://doi.org/10.1186/s12967-021-03159-9. Published 2021 Dec 7.

[60] L. Bai, L. Zhang, T. Pan, et al., Idiopathic pulmonary fibrosis and diabetes mellitus: a meta-analysis and systematic review, Respir. Res. 22 (1) (2021) 175, https://doi.org/10.1186/s12931-021-01760-6. Published 2021 Jun 8.

[61] S.G. Royce, V. Cheng, C.S. Samuel, M.L. Tang, The regulation of fibrosis in airway remodeling in asthma, Mol. Cell. Endocrinol. 351 (2) (2012) 167–175, https://doi.org/10.1016/j.mce.2012.01.007.

[62] M. Romagnoli, C. Nannini, S. Piciucchi, et al., Idiopathic nonspecific interstitial pneumonia: an interstitial lung disease associated with autoimmune disorders? Eur. Respir. J. 38 (2) (2011) 384–391, https://doi.org/10.1183/09031936.00094910.

[63] S. Palmucci, F. Galioto, G. Fazio, et al., Clinical and radiological features of lung disorders related to connective-tissue diseases: a pictorial essay, Insights Imaging 13 (1) (2022) 108, https://doi.org/10.1186/s13244-022-01243-2. Published 2022 Jun 29.

[64] A. Yoshizaki, Y. Iwata, K. Komura, et al., CD19 regulates skin and lung fibrosis via Toll-like receptor signaling in a model of bleomycin-induced scleroderma, Am. J. Pathol. 172 (6) (2008 Jun) 1650–1663, https://doi.org/10.2353/ajpath.2008.071049. Epub 2008 May 8. PMID: 18467694; PMCID: PMC2408424.

[65] K. Streicher, S. Sridhar, M. Kuziora, et al., Baseline plasma cell gene signature predicts improvement in systemic sclerosis skin scores following treatment with inebilizumab (MEDI-551) and correlates with disease activity in systemic lupus erythematosus and chronic obstructive pulmonary disease, Arthritis Rheumatol. 70 (12) (2018) 2087–2095, https://doi.org/10.1002/art.40656.

[66] Y. Liu, A. Beyer, R. Aebersold, On the dependency of cellular protein levels on mRNA abundance, Cell 165 (3) (2016) 535–550, https://doi.org/10.1016/j.cell.2016.03.014.

[67] M. Cinelli, S. Guiducci, A. Del Rosso, et al., Piascledine modulates the production of VEGF and TIMP-1 and reduces the invasiveness of rheumatoid arthritis synoviocytes, Scand. J. Rheumatol. 35 (5) (2006) 346–350, https://doi.org/10.1080/03009740600709865.

[68] I. Kholodnyuk, A. Kadisa, S. Svirskis, et al., Proportion of the CD19-positive and CD19-negative lymphocytes and monocytes within the peripheral blood mononuclear cell set is characteristic for rheumatoid arthritis, Medicina (Kaunas) 55 (10) (2019) 630, https://doi.org/10.3390/medicina55100630. Published 2019 Sep. 24.
[69] T.F. Tedder, CD19: a promising B cell target for rheumatoid arthritis, Nat. Rev. Rheumatol. 5 (10) (2009) 572–577, https://doi.org/10.1038/nrrheum.2009.184.
[70] L. Xiong, L. Xiong, H. Ye, et al., Animal models of rheumatoid arthritis-associated interstitial lung disease, Immun Inflamm Dis 9 (1) (2021) 37–47, https://doi.org/10.1002/iid3.377.